UNIVERSITÀ DEGLI STUDI DI PADOVA

Dipartimento di Biologia

Scuola di Dottorato di Ricerca in Biochimica e Biotecnologie

Indirizzo: Biotecnologie

Ciclo XXI

Prion protein: does N-terminal domain allow vesicular micronutrients uptake?

Direttore della Scuola: Ch.mo Prof. Giuseppe Zanotti

Supervisore: Ch.mo Prof. Benedetto Salvato

Dottorando: Marcello Ventura

Table of content

Abstract

Prion protein (PrP^C) is a cell surface glycoprotein, anchored by the GPI to the cell membrane. It seems to be involved in some neurodegenerative diseases, but its physiological function is still undefined. Many cellular functions were proposed as PrP^C roles, such as the modulation of several signal transduction pathways known to promote cellular survival and the protection against oxidative stress. Nevertheless, the main hypothesis on PrP^C role is in copper homeostasis.

Copper is an essential micronutrient (EMN) and all EMNs (vitamins and metals) are present in bodies and foods in micromolar concentrations. This feature can easily lead to deficiency. It is also clear that deficiency of EMNs produces overlapping diseases symptoms. Also the uptake pathway (endocytosis) is common for many EMN. Thanks to these reasons we hypothesize that prion protein could allow EMNs uptake.

The aim of this work is to study these binding processes and their characteristics. So N-terminal domain of mouse PrP^C ($mPrP^{23-109}$) was recombinant expressed and purified. To study specificity and characteristics of metals binding process, $mPrP^{23-109}$ was titrated with five first transition serie divalent metals (Mn, Co, Ni, Cu, Zn), at several pH values and it was followed in fluorescence spectroscopy. Furthermore, to define if metal binding could drive structural rearrangements in the prion protein N-terminal domain, we performed structural analysis using circular dicroism (CD). To investigate vitamins stacking between triptophan indolic rings, $mPrP^{23-109}$ was titrated with four vitamins belonging to B group and titrations were monitored by fluorescence anisotropy, that allows to know the fluorophores average molecular rotational speed. Finally, we also investigated the possibility that prion protein N-terminal domain could interact with membrane mimetic systems.

Our findings confirm that prion protein has a functional role in copper homeostasis. We also propose that prion protein, together with copper, plays a key role in integrated endocytic uptake pathway, involving all EMNs.

Riassunto

La protein prionica (PrP^C) è una glicoproteina legata alla superficie extracellulare della membrana tramite l'ancora GPI. Ad essa è stata attribuita la causa di alcune malattie neuro degenerative, ma la sua funzione fisiologica non è ancora stata definita. Molte funzioni sono state proposte, tra cui la modulazione di alcune vie di transduzione del segnale che promuovono la sopravvivenza cellulare e la protezione da stress ossidativo, ma l'ipotesi principale è una funzione nell'omeostasi del rame.

Il rame è un micro nutriente essenziale (MNE) e tutti gli MNE sono presenti nel corpo e negli alimenti in concentrazioni micromolari; ciò può determinare facilmente una deficinza. È ormai chiaro che i sintomi da deficienza sono comuni a molti MNE. Inoltre anche le vie di assorbimento di molti MNE sono analoghe fra loro, usando vie endocitiche. Grazie a queste evidenze abbiamo ipotizzato che la PrP^C possa essere coinvolta nell'assorbimento degli MNE.

Lo scopo di questo lavoro è di studiare questi legami e le loro caretteristiche. Per far ciò, è stato espresso e purificato il dominio N-terminale della proteina prionica di topo ($mPrP^{23-109}$). Per studiare la specificità e le caratteristiche del legame con i metalli, la proteina ricombinante è stata titolata con cinque metalli divalenti della prima serie di transizione (Mn, Co, Ni, Cu, Zn), a diversi valori di pH utilizzando la spettroscopia di fluorescenza. Per definire se le interazioni osservate fossero funzionali, è stata effettuata l'analisi strutturale in dicroismo circolare. Per verificare la proabile interazione tra le vitamine ed i triptofani della proteina, $mPrP^{23-109}$ è stata titolata con quattro vitamine, appartenenti al gruppo B, ed è stata monitorata la velocità dei fluorofori mediante l'anisotropia di fluorescenza. Infine è stata anche studiata l'interazione tra dominio N-terminale della PrP^C con sistemi mietici di membrane.

I nostri risultati confermano che la PrP^C ha un ruolo funzionale nell'omeostasi del rame. Inoltre proponiamo che la proteina prionica, insieme con il rame, ricopre un ruolo chiave nell'assorbimento integrato degli MNE, via endocitosi.

1. Introduction

1.1. Prion protein

1.1.1. Prion diseases

Prion diseases are a group of fatal neurodegenerative disorders. In table 1 are listed some of these diseases[1].

The history of prion diseases began in nineteen twenties when Creutzfeldt and Jakob described a clinically polymorphic cerebral syndrome. In 1957 Gajdusek and Zigas described the kuru disease in a group of cannibals indigenous in Papua. In 1960s John Stanley Griffith developed the "protein only" hypothesis. Finally, in 1982 Stanley B. Prusiner announced the purification of the hypothetical infectious agent, called Prion. The specific protein that constitutes the prion was named PrP (Protease resistant Protein).

DISEASE	ABBREVIATION	NATURAL HOST
Kuru		Human
Creutzfeldt-Jakob disease	CJD	Human
Gerstmann-Sträussler-Scheinker syndrome	GSS	Human
Fatal familial insomnia	FFI	Human
Scrapie		Sheep, goat and mouflon
Bovine spongiform encephalopathy	BSE	Cattle
Chronic wasting disease	CWD	Deer and elk
Exotic ungulate encephalopathy	EUE	Nyala, kudu and oryx
Feline spongiform encephalopathy	FSE	Felines in captivity
Transmissible mink encephalopathy	TME	Mink (farm raised)

Table 1: Prion diseases.

The "protein-only" hypothesis affirms that the infectious prion pathogen agent consists only of the abnormal prion protein, PrP^{Sc}. This protein is an altered isoform of a normal cellular protein, PrP^{C}, which is host encoded by a chromosomal gene and abundantly expressed in mammalian cells. Furthermore, the two prion protein

isoforms have different physical properties. PrP^{C} exists as a monomer that is readily degradable by proteinase K, whereas PrP^{Sc} forms insoluble aggregates that show high resistance to proteinase K digestion and often have the characteristics of an amyloid[1]. The covalent structure of PrP^{Sc} is most likely identical with that of PrP^{C} [2].
The mechanism of PrP^{C}- PrP^{Sc} conversion and PrP^{Sc} toxicity is still undefined.

1.1.2. Sequence and structural features of human PrP^{C}

The human PrP^{C} mRNA translation is a 253 aminoacid polypeptide (254 in mouse). First 22 residues are the leader sequence to endoplasmic reticulum (ER) and it is cleaved after reaching ER. The last 23 aminoacids (24 in mouse) are the signal peptide to the attachment of a glycosylphosphatidylinositol (GPI) anchor to serine 230[3]. Further posttranslational processes are two N-linked glycosilations (Asn181 and Asn197) and one disulfide bond (Cys179 and Cys214)[2].
Mature PrP^{C} (figure 1) is a cell surface 208 residue glycoprotein anchored by the GPI to the cell membrane. It is composed by two distinct domains, the N-terminal and C-terminal domains.
The N-terminal half of the protein (residues 23–125) is random coiled[4], with considerable backbone flexibility[5]. Residues 51–91 constitute of the so called octarepeat region; four of which (residues 60–91) have the sequence $(PHGGGWGQ)_4$, that bind cooperatively copper ions[6; 7; 8]; the last one (residues 51–59) have a homologous sequence but lack the histidine residue (PQGGGGWGQ). It is called the 5th site[7; 9; 10; 11; 12; 13], that has a lower copper affinity.
The C-terminal domain (residues 126-231) is a globular structure, comprising three α-helices and two short β-strands[4; 14; 15].

1.1.3. Tissue expression, cellular localization and traffiking

PrP^{C} is expressed most abundantly in neurons[16] and glial cells[17], but has also been detected in other non neuronal tissues, as lymphoid cells, lung, heart, kidney, gastrointestinal tract, muscle, and mammary glands[18].

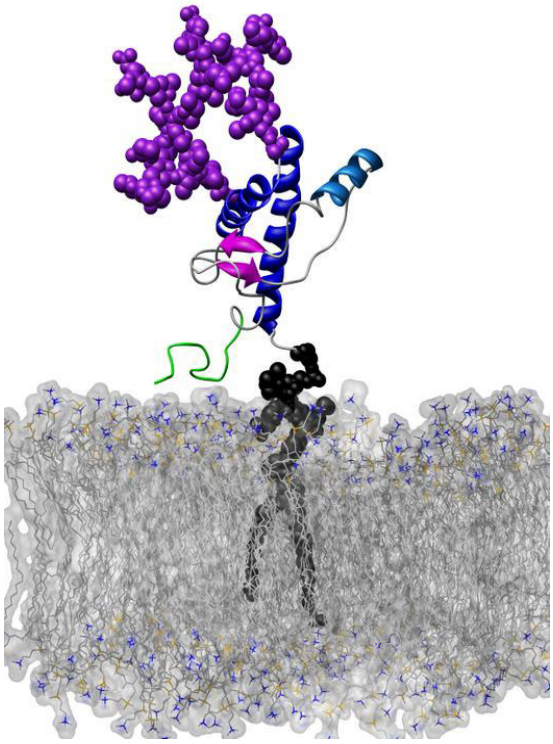

Figure 1: Theoretical physiological PrP^C on membrane.

PrP^C is a cell surface glycoprotein, however cytosolic localized PrP has also been detected[19].

PrP^C is found in caveolae like domains both at the transgolgi network, at plasma membrane and in interconnecting chains of endocytic caveolae like domains[20; 21]. These microdomains are enriched in cholesterol and they are called lipid rafts[20].

Trafficking of PrP^C seems to be a complex cellular event and may involve more than one internalization mechanism.

Like several GPI anchored proteins which lack cytoplasmatic domains, PrP^C seems to be internalized through caveolae in a raft dependent mechanism[22; 23]. It is delivered to the pericentriolar region via caveolae containing early endocytic structures to late endosomes or lysosomes[21].

Furthermore that PrP^C traffics through the Golgi complex, plasma membrane and early recycling endosomes. These observations indicate that traffic of PrP^C is not determined predominantly by the GPI anchor and that, differently from other GPI

anchored proteins, PrP^C is delivered to classic endosomes after internalization via clathrin dependent endocytosis[24; 25].

It can be concluded that cell surface PrP^C constitutively cycles between the plasma membrane and early endosomes via a clathrin or caveolin dependent mechanism.

1.1.4. Phylogenesis

Genes encoding homologous prion proteins have been reported in all tetrapod groups and in lower vertebrates (figure 2).

Analysis of primary amino acid sequences indicates strong structural conservation in evolution[26], suggesting important biological roles for the protein, in spite 3D structure data are available only for some mammalian prion proteins.

Figure 3 shows that the repetitive N-terminal domain within each vertebrate class contains a distinctive default number of degenerate repeats that share the same tetrapeptide as a basic unit. From fish to human, the repeat units within one molecule have reduced in degeneracy, possibly by gene conversion and homogenization, and have increased their size in discrete steps, reaching a maximum of eight amino acids in mammals[27].

Inter-group comparisons among mammalian, avian, reptile and amphibian polypeptides reveal a sharp decrease in sequence identity, without loss of structural similarity. Therefore, homology between distantly related prion proteins must be proposed using a minimum set of structural landmarks and not only basing on sequence similarity. Accordingly, although the 461 residues fish prion polypeptide (Fugu PrP^{461}) is only 22% similar in primary sequence to mammalian prions, it contains the characteristic N-terminal repetitive stretch, a hydrophobic motif and a C-terminal globular domain. Moreover, 3D structural modelling predicts strong conservation of tertiary structure between Fugu PrP^{461}, zebrafish PrP and human PrP^C (figure 4)[26; 27].

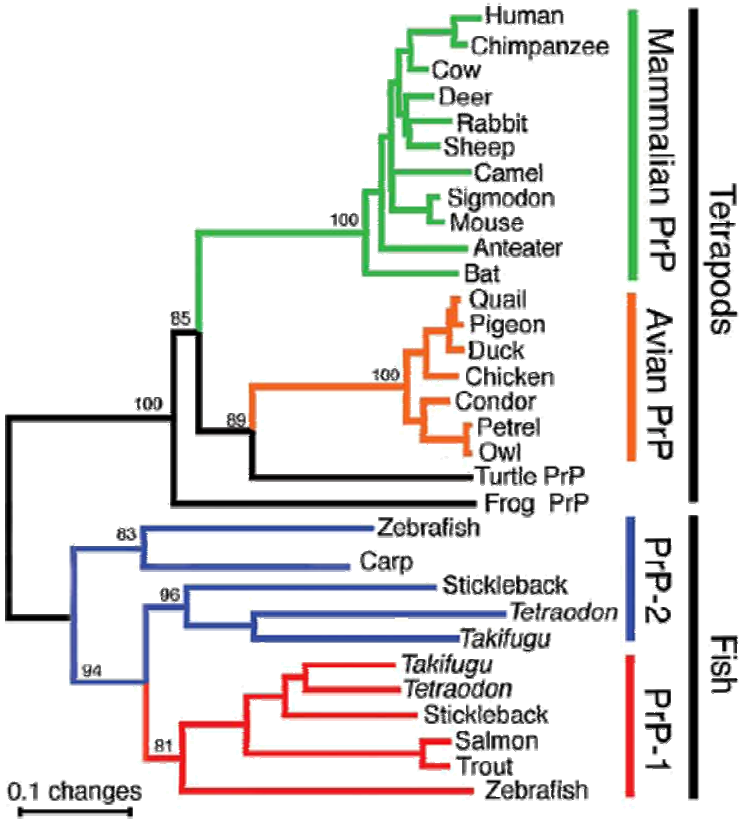

Figure 2: Phylogenetic tree of PrP^{C} [26].

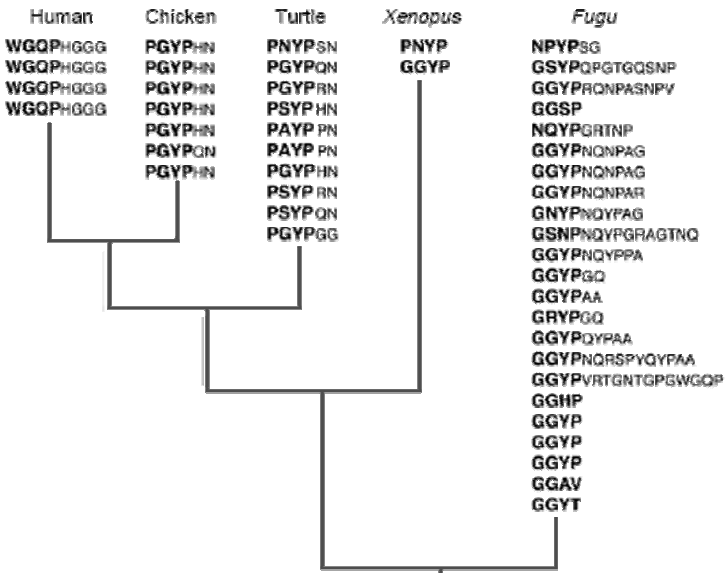

Figure 3: Phylogenetic tree of PrP^{C} repetitive N-terminal domain[27].

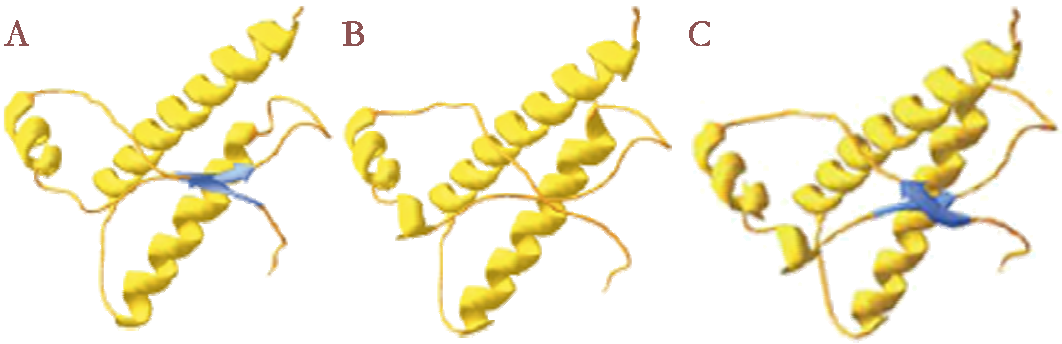

Figure 4: C-terminal tridimensional structures: panel A, human PrP^{C}; panel B, Fugu PrP^{461}; panel C, zebrafish $PrP^{26; 27}$

These data demonstrate that vertebrate N-terminal and C-terminal domains evolved as two separate modules, which strongly implies at least two very different functional properties of the native molecule.

1.1.5. Putative physiological roles

Cellular prion protein (PrP^{C}) physiological function remains ambiguous. It seems to be involved in different cellular processes, such as the regulation of cell death[28; 29; 30], the protection against oxidative stress[31; 32] and the modulation of several signal transduction pathways known to promote cellular survival[33; 34; 35].

Although all these hypotheses are well documented, the main PrP^{C} feature is N-terminal copper binding and, accordingly, copper homeostasys is one of the most important hypothesized function. There are many important facts that support this role.

First, copper binding to the octarepeat region reversibly stimulates endocytosis of PrP^{C} from the cell surface, suggesting PrP^{C} acts as a receptor for cellular uptake or efflux of copper[36; 37; 38; 39].

It has been described that cerebellar cells from PrP^{C} knockout mice contain only 20% of copper amount present in cells from wild type animals[6], and highlighted sensitivity to Cu^{2+} induced oxidative stress[40; 41]. As mentioned above, PrP^{C} is high concentrated at presynaptic membranes in the central nervous system, where Cu^{2+} is

also highly localized[42]. These data suggest that PrP^{C} is an important copper binding protein in the brain.

In addition, the octarepeat region of the human PrP^{C} ($PrP^{59–91}$) reduces Cu^{2+} to Cu^{1+} in vitro, which depends on the tryptophan residues present in the octapeptide repeats[43; 44; 45].

1.2. Transition metals

1.2.1. Manganese (Mn)

1.2.1.1. Biological function

Manganese is an essential nutrient involved in the formation of bone and in amino acid, cholesterol, and carbohydrate metabolism. This element appears to be essential in trace amounts to all forms of life. Manganese metalloenzymes include arginase, glutamine synthetase, phosphoenolpyruvate decarboxylase, and manganese superoxide dismutase. Glycosyltransferases and xylosyltransferases, which are important in proteoglycan synthesis and thus bone formation, are sensitive to manganese status in animals. Several other manganese-activated enzymes, including pyruvate carboxylase, can also be activated by other ions, such as magnesium.

1.2.1.2. Physiology of Absorption, Metabolism, and Excretion

Only a small percentage of dietary manganese is absorbed.

Studies in Caco-2 cells[46], an in vitro model of the gastrointestinal epithelium, reveal that iron (Fe) treatment decreases cellular uptake of Fe, Mn, and zinc (Zn), suggesting that these metals may utilize the same apical and basolateral transporters. Carrier-mediated Mn transport has been demonstrated in Caco-2 cells from the apical side[47]. There is evidence that divalent metal transporter (DMT-1) transports Mn(II) at the cell membrane[48] or translocates it from endocytosed vesicles. Intestinal ^{54}Mn absorption in Belgrade omozygous b/b rats, that do not express a significant amount of functional DMT1 protein, was 40% of that seen in heterozygous +/b

rats, which are phenotypically normal[49]. On the contrary, Crossgrove and Yokel say that DMT1 is not a major mechanism of the carrier mediated uptake of Mn into brain at the blood brain barrier (BBB)[50]. Carrier-mediated Mn transport has been demonstrated also in cultured brain endothelial cells[51] and in astrocytes[52]. The precise transporter for Mn into astrocytes is unknown; however, it has been suggested that transferrin receptor (TfR) and/or DMT1 proteins may be important[53]. Brain entry of the Mn(II) ion, Mn transferrin (Mn Tf) and Mn citrate across the BBB is transporter mediated[54, 55, 56].

Manganese is taken up from the blood by the liver and transported to extrahepatic tissues by transferrin[57] and possibly α2-macroglobulin[56] and albumin[58]. Manganese inhibited iron absorption, both from a solution and from a hamburger meal[59]. Glial cells, particularly astrocytes represent the brain manganese reserve[60], with concentrations 10–50 folds greater than in neurons.

Absorbed manganese is excreted very rapidly into the gut via bile[61], so this metal is excreted primarily in feces. Urinary excretion of manganese is low and has not been found to be sensitive to dietary manganese intake[58].

1.2.2. Cobalt (Co)

1.2.2.1. Biological function

Cobalt is an essential nutrient involved in protein synthesis and in cobalamin (vitamin B_{12}) structure.

Vitamin B_{12} is a cofactor for a number of enzymes[62].

Methionyl aminopeptidase, which catalyzes the removal of the initiator methionine from nascent polypeptide chains, contains cobalt ions in both prokaryotes and eukaryotes[62; 63, 64].

1.2.2.2. Physiology of Absorption, Metabolism, and Excretion

Microorganisms are the only natural sources of the B_{12} derivatives, whereas most spheres of life (except for the higher plants) depend on these[65].

Little is known about Co metabolism in humans.

There is evidence that DMT1 transports Co in many mammalian tissues, including intestine[48].

It is been reported that cobalt could be uptaked by cells also *via* transferrin receptor (TfR)[66].

1.2.3. Nickel (Ni)

1.2.3.1. Biological function

There have been no studies to determine the nutritional importance of nickel in humans, nor has a biochemical function been clearly demonstrated for nickel in higher animals or humans[67]. Nickel may serve as a cofactor or structural component of specific metalloenzymes of various functions, including hydrolysis and redox reactions and gene expression[68; 69]. Nickel may also serve as a cofactor facilitating ferric iron absorption or metabolism[70]. Nickel is an essential trace element in animals, as demonstrated by deficiency signs reported in several species. Rats deprived of nickel exhibit retarded growth, low hemoglobin concentrations[71] and impaired glucose metabolism[72]. Nickel may interact with the vitamin B_{12}- and folic acid-dependent pathway of methionine synthesis from homocysteine[73].

1.2.3.2. Physiology of Absorption, Metabolism, and Excretion

The absorption of dietary nickel is typically less than 10 percent[74].

The mechanism by which nickel is taken up from the diet into the enterocyte and further into the circulation is not known, but results obtained with isolated small intestinal segments of rats and monolayers of human intestinal Caco2 cells indicate that nickel and iron share and compete for absorptive pathways[75; 76; 77]. DMT1 has been shown to be present in the apical membrane of enterocytes and it was been demonstrated to mediate influx of a wide range of divalent metal ions into these cells[48; 78].

Nickel is transported in blood bound primarily to albumin[79]. Although most tissues and organs do not significantly accumulate nickel, in humans the thyroid and adrenal glands have relatively high nickel concentrations[80].

Because of the poor absorption of nickel, the majority of ingested nickel is excreted in the feces, and the majority of absorbed nickel is excreted in the urine with minor amounts excreted in sweat and bile.

1.2.4. Copper (Cu)

1.2.4.1. Biological function

The biochemical role for copper is primarily catalytic, with many copper metalloenzymes acting as oxidases to achieve the reduction of molecular oxygen. Many copper metalloenzymes have been identified in humans.

Amine oxidases participate in important reactions that have markedly different effects. Diamine oxidase inactivates histamine released during allergic reactions. Monoamine oxidase (MAO) is important in serotonin degradation to excretable metabolites and in the metabolism of catecholamines (epinephrine, norepinephrine, and dopamine). Lysyl oxidase uses lysine and hydroxylysine found in collagen and elastin as substrates for post-translational processing to produce cross-linkages needed for the development of connective tissues, including those of bone, lung, and the circulatory system.

Ferroxidases are copper enzymes found in plasma, with a function in ferrous iron oxidation (Fe(II)→Fe(III)) that is needed to achieve iron's binding to transferrin[81]. Ferroxidase I, also called ceruloplasmin, is the predominant copper protein in plasma and may also have antioxidant functions. Defects in ceruloplasmin function produce cellular iron accumulation, a result that supports its ferroxidase role[82].

Cytochrome C oxidase is a multisubunit enzyme in mitochondria that catalyzes reduction of O_2 to H_2O. This establishes a high energy proton gradient required for adenosine triphosphate (ATP) synthesis. This copper enzyme is particularly abundant in tissues of greatest metabolic activity including heart, brain, and liver.

Two forms of superoxide dismutase are expressed in mammalian cells, a mangano and cupro/zinc form. Copper/zinc superoxide dismutase (Cu/Zn SOD) uses two copper atoms for conversion of the superoxide anion (O_2^-) to H_2O_2 and O_2. Zinc atoms have a structural role in the enzyme. The enzyme is localized in the cytosol and, along with the mitochondrial manganese-containing form, provides a defense against oxidative damage from superoxide radicals that, if uncontrolled, can lead to other damaging reactive oxygen species. Mutations in the Cu/Zn SOD gene, which alter the protein's redox behavior, produce amyotrophic lateral sclerosis (Lou Gehrig's disease).

There is substantial documentation from animal studies that diets low in copper reduce the activities of many of these copper metalloenzymes. Activities of some copper metalloenzymes have been shown to decrease in human copper depletion[83]. Physiologic consequences resulting from copper deficiency include defects in connective tissue that lead to vascular and skeletal problems, anemia associated with defective iron utilization, and possibly specific aspects of central nervous system dysfunction. Some evidence suggests that immune and cardiac dysfunction occurs in experimental copper deficiency and the development of such signs of deficiency has been demonstrated in infants[84; 85].

1.2.4.2. Physiology of Absorption, Metabolism, and Excretion

Metabolism of copper in humans relies on the intestine for control of homeostasis as the capacity for renal copper excretion is limited. Nearly two-thirds of the body copper content is located in skeleton and muscle, but studies with stable isotopes have shown that the liver is a key site in maintaining plasma copper concentrations[85; 86]. Copper has a higher binding affinity for proteins than all other divalent trace elements. Consequently, precise control of intracellular copper trafficking is needed to regulate how it is donated to appropriate sites.

Copper absorption occurs primarily in the small intestine.

The Human Copper Transporter (hCtr) Family proteins are the main transporter for copper. These proteins have three putative transmembrane regions. The N-terminal

region of hCtr1 possesses two methionine-rich regions, known as "Mets" motifs[87] and the C-terminus contain a sequence of conserved cysteine and histidine[88] (figure 5, panel A).

Human high-affinity Ctr1, a homotrimeric complex, is thought to provide a channel enabling the passage of copper across the lipid bilayer (figure 5, panel B). Moreover hCtr1-mediated copper uptake occurs with a millimolar Km and the preferred

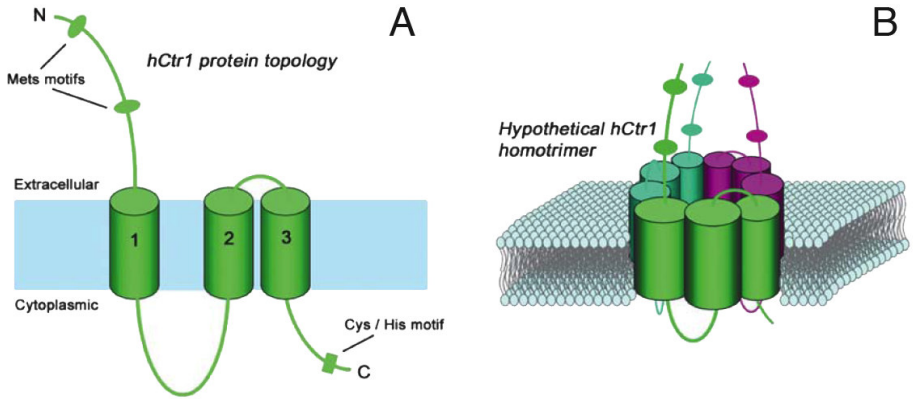

Figure 5: Topological model for the structure of the hCtr1 protein. The features, common to Ctr1 family members, include three predicted transmembrane domains, an extracellular amino terminal region containing two methionine rich (Mets) motifs and a putative cytoplasmic carboxyl terminal region containing a Cys/His motif (panel A). Also shown is a hypothetical model depicting a transmembrane channel formed by the trimerization of hCtr1.[89]

substrate is reduced Cu(I), taked up by an energy-independent mechanism stimulated by extracellular acidic pH[90]. The mouse Ctr1 transporter is essential for Cu(I) homeostasis and embryonic development[91; 92].

Indirect immunofluorescence experiments with cultured cells suggest hCtr1 is located in perinuclear vesicles and at the plasma membrane[90; 93].

Mammals possess additional functional copper transport activities. The divalent metal transporter-1 (DMT1), was considered a possible candidate for this alternative copper transport activity[94].

Copper trafficking to the secretory pathway for efflux from cells is mediated by the Menkes P-type ATPase (MNK; ATP7A)[82].

Copper is released *via* plasma to extrahepatic sites where up to 95 percent of the copper is bound to ceruloplasmin.

Other P-type ATPases (Wilson; ATP7B) are responsible for copper trafficking to the secretory pathway for ceruloplasmin synthesis or for endosome formation before transport into the bile[82; 95]. Mutations of this copper-transporting ATPase result in cellular copper accumulation called Wilson's disease.

Biliary copper excretion is adjusted to maintain balance.

Urinary copper excretion is normally very low over a wide range of dietary intakes. As with other trace elements, renal dysfunction can lead to increased urinary losses.

1.2.5. Zinc (Zn)

1.2.5.1. Biological function

Zinc is the second most abundant metallic element in the body, following iron. It has been shown to be essential for microorganisms, plants, and animals. Zinc is an essential micronutrient that plays fundamental roles in physiology, cellular metabolism and gene expression. Zn is required as a catalytic cofactor of more than 300 enzymes and it stabilizes the structure of thousands of protein domains.

Examples of zinc metalloenzymes can be found in all six enzyme classes[96]. Well-studied zinc metalloenzymes include the ribonucleic acid (RNA) polymerases, alcohol dehydrogenase, carbonic anhydrase and alkaline phosphatase. Zinc is defined as a Lewis acid, and its action as an electron acceptor contributes to its catalytic activity in many of these enzymes.

The structural role of zinc involves proteins that form domains capable of zinc coordination, which facilitates protein folding to produce biologically active molecules. The vast majority of such proteins form a "zinc finger like" structure created by chelation centers, including cysteine and histidine residues[97]. Some of these proteins have roles in gene regulation as DNA binding transcription factors. Zinc also provides a structural function for some enzymes; copper-zinc superoxide dismutase is the most notable example. Also of potential relevance as a structural role

is the essentiality of zinc for intracellular binding of tyrosine kinase to T-cell receptors, CD4 and CD8α, which are required for T-lymphocyte development and activation[98; 99].

While knowledge of the biochemical and molecular genetics of zinc function is well developed and expanding, neither the relationship of these genetics to zinc deficiency or toxicity nor the functions for which zinc is particularly critical have been established. For example, explanations for depressed growth, immune dysfunction, diarrhea, altered cognition, host defense properties, defects in carbohydrate utilization, reproductive teratogenesis, and numerous other clinical outcomes of mild and severe zinc deficiency have not been conclusively established.

1.2.5.2. Physiology of Absorption, Metabolism, and Excretion

Zinc is widely distributed in foods. Because virtually none of it is present as the free ion, bioavailability is a function of the extent of digestion. Digestion produces the opportunity for zinc to bind to exogenous and endogenous constituents in the intestinal lumen, including peptides, amino acids, nucleic acids, and other organic acids and inorganic anions such as phosphate. The vast majority of zinc is absorbed by the small intestine through a transcellular process with the jejunum being the site with the greatest transport rate[100; 101].

Zn is highly charged and cannot cross biological membranes by passive diffusion, requiring the aid of a set proteins, grouped into two families on the basis of their structural and functional features: Solute Carrier Family 39A (SLC39A) includes mammalian ZRT/IRTrelated proteins (ZIPs)[102], and Solute Carrier Family 30A (SLC30A), comprises mammalian ZnTs[103]. Both ZIPs and ZnTs are multipass transmembrane proteins and have a high content of lipophilic amino acids. Fourteen ZIP-encoding genes have been identified in the human genome and are grouped into four sub-families according to the molecular features of the encoded proteins. All of the Zip proteins mediate Zn uptake from the extracellular environment or intracellular vesicles into the cytoplasm. Proteins belonging to the ZnT family were shown to be responsible for Zn efflux from the cytoplasm towards either

intracellular vesicles or/and the extracellular space[104], as well as for Zn delivery to specific metalloproteins[105]. Mutations in two Zn transporters have been linked to the Zn deficiency diseases acrodermatitis enteropathica (ZIP4) in humans[106]. A point mutation in ZnT2 was recently associated with transient Zn deficiency in exclusively breast-fed infants[107].

Considerable amounts of zinc enter the intestine from endogenous sources. Homeostatic regulation of zinc metabolism is achieved principally through a balance of absorption and secretion of endogenous reserves involving adaptive mechanisms programmed by dietary zinc intake. Over 85 percent of the total body zinc is found in skeletal muscle and bone. While plasma zinc is only 0.1 percent of this total, its concentration is tightly regulated at about 10 to 15 μmol/L.

Albumin is the principal zinc-binding protein in plasma from which most metabolic zinc flux occurs. Plasma amino acids bind some zinc and could be an important source of zinc excretion.

Metallothioneins (MTs) are small cytosolic proteins with a high cysteine content that bind Zn, as well as other metal ions, with high affinity. MTs were the first group of proteins involved in Zn homeostasis to be identified and extensively studied. MTs are thought to be responsible for the intracellular regulation of Zn concentration and for detoxification of non-essential heavy metals[108].

Zinc secretion into and excretion from the intestine provides the major route of endogenous zinc excretion. It is derived partially from pancreatic secretions, which are stimulated after a meal. Biliary secretion of zinc is limited, but intestinal cell secretions also contribute to fecal loss. Urinary zinc losses are only a fraction (less than 10 percent) of normal fecal losses.

1.3. Water soluble vitamins

Water soluble vitamins represent a group of structurally and functionally unrelated compounds that share a common feature of being essential for normal health and well being. These micronutrients play critical roles in manteining normal methabolic,

energy, differentiation and growth status of mammalian cells. Because mammals cannot synthetize these compounds, except for some synthesis of niacin, they must obtain them from two exogenous sources: a dietary source, preferentially uptaked in the small intestine, and a microflora bacterial source, uptaked in the large intestine.

1.3.1. Vitamin B1 (thiamine)

1.3.1.1. Biological function

Vitamin B1, also known as Thiamine, was the first B vitamin identified.

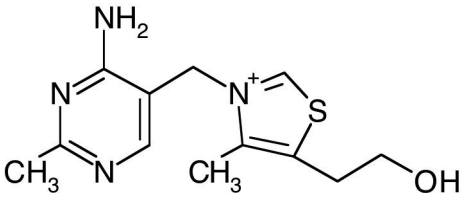

Figure 6: chemical structure of vitamin B1

Thiamine exists mainly in various interconvertible phosphorylated forms, chiefly thiamine pyrophosphate (TPP). TPP, the coenzymatic form of thiamine, is involved in two main types of metabolic reactions: decarboxylation of α-ketoacids, like pyruvate and α-ketoglutarate, and transketolation, for example among hexose and pentose phosphates.

Chemically, thiamine consists of substituted pyrimidine and thiazole rings linked by a methylene bridge (figure 6).

Thiamin deficiency causes *beriberi* that leads to a variety of clinical abnormalities, including neurological and cardiovascular disorders[109; 110].

1.3.1.2. Physiology of Absorption, Metabolism, and Excretion

Following ingestion, absorption of thiamine occurs mainly in the jejunum.

Thiamin uptake in the human intestine occurs via a specialized carrier-mediated mechanism and is pH-dependent, suggesting a thiamine/H^+ exchange mechanism[111]. The molecular identity of the systems involved has been identified as members of the monocarboxylate transporter gene family SLC16. Both of the human thiamin transporters (hTHTRs) hTHTR1 and hTHTR2 were found to be expressed in the human intestine[112; 113; 114; 115].

Thiamine is transported in blood both in erythrocytes and plasma.

Only a small percentage of a high dose of thiamine is absorbed, and elevated serum values result in active urinary excretion of the vitamin[116].

1.3.2.Vitamin B2 (riboflavin)

1.3.2.1. Biological function

Subsequent to the discovery of thiamine was the discovery of a more heat-stable factor that was named vitamin B2, or riboflavin (figure 7).

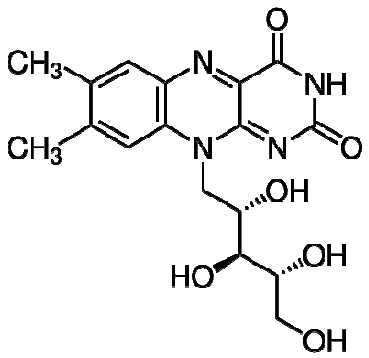

Figure 7: chemical structure of vitamin B2

The primary form of the vitamin is as an integral component of the coenzymes flavin mononucleotide (FMN) and flavin-adenine dinucleotide (FAD)[117; 118]. It is in these bound coenzyme forms that riboflavin functions as a catalyst for redox reactions in numerous metabolic pathways and in energy production.

The redox reactions in which flavocoenzymes participate include flavoprotein-catalyzed dehydrogenations that are both niacin dependent and independent, reactions with sulfur-containing compounds, hydroxylations, oxidative decarboxylations, dioxygenations, and reduction of oxygen to hydrogen peroxide.
Deficiency of riboflavin in humans leads to several symptoms including degenerative changes in nervous system, skin disorders and anemia.

1.3.2.2. Physiology of Absorption, Metabolism, and Excretion

Most dietary riboflavin is consumed as a complex of food protein with FMN and FAD[118]. In the stomach, gastric acidification releases most of the coenzyme forms of riboflavin (FAD and FMN) from the protein. The noncovalently bound coenzymes are then hydrolyzed to riboflavin by nonspecific pyrophosphatases and phosphatases in the upper gut[117; 118].

A vast amount of research defined the regulatory mechanisms involved in riboflavin transport across different cell line models. Althought kinetic parameters defere, it was showed the riboflavin uptake mechanism is highly specific and saturable and the primary absorption occurs in the proximal small intestine[117; 118; 119]. There are findings suggesting riboflavin transport involves carrier-mediated transport and receptor-mediated endocytosis[120; 121; 122].

Recently a human riboflavin transporter (hRFT1) was successfully identified. The tissue distribution, cellular localization, and functional characterization suggested that hRFT1 plays an important role in the cellular uptake of riboflavin. The high levels of hRFT1 in the small intestine and colon suggest that hRFT1 mediates the absorption of riboflavin at these sites. In addition, it was independent of Na^+, membrane potential or pH[123].

In plasma some riboflavin is complexed with albumin; however, a large portion of riboflavin associates with other proteins, mainly immunoglobulins, for transport[124].

The metabolism of riboflavin is a tightly controlled process that depends on the riboflavin status of the individual[125]. Riboflavin is converted to coenzymes within the cellular cytoplasm of most tissues but mainly in the small intestine, liver, heart, and

kidney. The metabolism of riboflavin begins with the ATP-dependent phosphorylation of the vitamin to FMN. Flavokinase, the catalyst for this conversion, is under hormonal control. FMN can then be complexed with specific apoenzymes to form a variety of flavoproteins; however, most is converted to FAD by FAD synthetase. As a result, FAD is the predominant flavocoenzyme in body tissues. Production of FAD is controlled by product inhibition such that an excess of FAD inhibits its further production[126].

When riboflavin is absorbed in excess, very little is stored in the body tissues. The excess is excreted, primarily in the urine. A wide variety of flavin related products have been identified in the urine of humans[127].

1.3.3.Vitamin B3 (niacin)

1.3.3.1. Biological function

Vitamin B3, or niacin, refers to nicotinamide (nicotinic acid amide), nicotinic acid (pyridine-3-carboxylic acid), and derivatives that exhibit the biological activity of nicotinamide (figure 8).

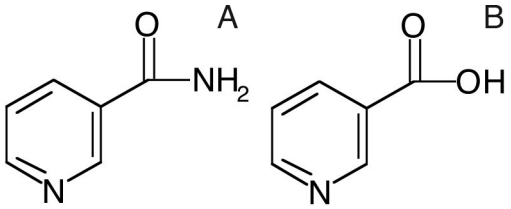

Figure 8: chemical structure of vitamin B3 (A: nicotinamide; B: nicotinic acid)

The nicotinamide moiety of the pyridine nucleotide coenzymes, nicotinamide adenine dinucleotide (NAD) and nicotinamide adenine dinucleotide phosphate (NADP), acts as a hydride ion acceptor or donor in many biological redox reactions. NAD has also been shown to be required for important nonredox adenosine

diphosphate (ADP) ribose transfer reactions involved in DNA repair and calcium mobilization[128; 129].

NAD functions in intracellular respiration and as a codehydrogenase with enzymes involved in the oxidation of fuel molecules such as glyceraldehyde 3-phosphate, lactate, alcohol, 3-hydroxybutyrate, pyruvate, and α-ketoglutarate. NADP functions in reductive biosyntheses such as in fatty acid and steroid syntheses and, like NAD, as a codehydrogenase as in the oxidation of glucose 6-phosphate to ribose 5-phosphate in the pentose phosphate pathway.

Deficiency of niacin leads to pellagra, a disease characterized by skin lesions, dermatitis, ataxia and dementia.

1.3.3.2. Physiology of Absorption, Metabolism, and Excretion

The human body obtains niacin from two sources: an endogenous one in which the vitamin is produced by methabolic conversion of tryptophan to niacin, and an exogenous one from the diet *via* absorption in the intestine. Glycohydrolases in the intestine catalyze the release of nicotinamide from NAD[130].

The mechanism of uptake of dietary niacin (nicotinic acid) by intestinal epithelial cells is not well understood, and nothing is known about regulation of the uptake process. There is evidence that another member of the monocarboxylate transporter gene family SLC16, MCT1, is capable of transporting nicotinic acid. This mechanism involves electroneutral co-transport of nicotinate and H^+[131; 132; 133]. There is also an evidence for the presence of a Na^+-coupled transport system for nicotinate and the structurally related compound pyrazinoate[134; 135; 136].

The niacin coenzymes NAD and NADP are synthesized in all tissues of the body from nicotinic acid or nicotinamide. Tissue concentrations of NAD appear to be regulated by the concentration of extracellular nicotinamide, which in turn is under hepatic control and is hormonally influenced. Hydrolysis of hepatic NAD allows the release of nicotinamide for transport to tissues that lack the ability to synthesize the NAD and NADP coenzymes from tryptophan. In the liver some excess plasma nicotinamide is converted to storage NAD. Tryptophan and nicotinic acid also

contribute to storage NAD following the biosynthetic pathway, going through pyridine mononucleotide (NAMN), which is then reamidated to NAD. In the degradation of NAD, the nicotinamide formed can be reconverted to NAD via nicotinamide ribonucleotide. Nicotinamide can be deamidated in the intestinal tract by intestinal microflora[137].

Excess niacin is methylated in the liver to N1-methyl-nicotinamide, which is excreted in the urine. The two major excretion products are N1-methyl-nicotinamide and its pyridone derivative[138].

1.3.4.Vitamin B6

1.3.4.1. Biological function

Vitamin B6 (figure 9) comprises a group of six related compounds: pyridoxal (PL), pyridoxine (PN), pyridoxamine (PM), and their respective 5'-phosphates (PLP, PNP, and PMP).

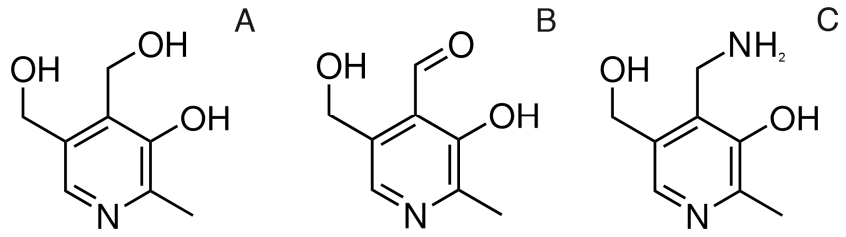

Figure 9: chemical structures of vitamin B6 (A: PN; B: PL; C: PM)

PLP is a coenzyme for more than 100 enzymes involved in amino acid metabolism, including aminotransferases, decarboxylases, racemases, and dehydratases. Examples are δ-aminolevulinate synthase, which catalyzes the first step in heme biosynthesis, cystathionine β-synthase and cystathioninase, enzymes involved in the transsulfuration pathway from homocysteine to cysteine. For practically all PLP enzymes the initial step in catalysis involves formation of a Schiff's base between an incoming amino acid, *via* its α-amino group, and the carbonyl group of PLP.

1.3.4.2. Physiology of Absorption, Metabolism, and Excretion

In animal tissue the major forms of vitamin B6 are PLP and PMP. Absorption in the gut involves phosphatase mediated hydrolysis followed by transport of the nonphosphorylated form into the mucosal cell.

Experiments on Caco-2 cells indicate that vitamin B6 uptake occurs *via* a specialized, carrier-mediated mechanism, that is pH dependent. Uptake was found to be higher at acidic pH than alkaline conditions. Also for this vitamin, authors suggest that the transport of pyridoxine may be occurring via a pyridoxine/H^+ symport mechanism[139].

Others experiments on cultured mouse colonic cells and native human colonic vescicles show the existence of a specific carrier-mediated mechanism for pyridoxine; conversely to the previous, uptake was found to be higher at neutral/alkaline pH compared with acidic conditions[140].

However, the precise transporter has not yet been identified.

Most of the absorbed nonphosphorylated vitamin B6 goes to the liver, where PN, PL, and PM are phosphorylated by PL kinase. PNP, which is normally found only at very low concentrations, and PMP are oxidized to PLP by PNP oxidase. PMP is also generated from PLP via aminotransferase reactions. PLP is bound to various proteins in tissues; this protects it from the action of phosphatases. The capacity for protein binding limits the accumulation of PLP by tissues at very high intakes of B6[141]. When this capacity is exceeded, free PLP is rapidly hydrolyzed and nonphosphorylated forms of B6 are released by the liver and other tissues into circulation.

PLP is the major form of the vitamin in plasma and is derived entirely from liver as a PLP-albumin complex[142; 143]. Tissues and erythrocytes can transport nonphosphorylated forms of the vitamin from plasma. Some of this is derived from plasma PLP after phosphatase action. In tissues, conversion of the transported vitamin to PLP, coupled with protein binding, allows accumulation and retention of

the vitamin. B6 in tissues is found in various subcellular compartments but primarily in the mitochondria and the cytosol.

PLP in the liver can be oxidized to 4-pyridoxic acid (4-PA), which is released and excreted.

2. Aim of the work

It is now becoming clear that prion diseases are caused by a fact that perturbs the normal, physiological activity of PrP^C.

An alternative hypothesis for prion toxicity postulates that PrP^C possesses a biological activity that, when lost, would cause neurodegeneration[144]. It is also known that genetic ablation of PrP expression, either prenatally[145; 146] or postnatally[147], has relatively little phenotypic effect and does not produce any features of a prion disease. Thus, loss of PrP^C function cannot, by itself, account for prion induced neurodegeneration.

Our hypothesis on PrP^C physiological role is partially in agreement with this theory. Loss of protein function can be caused by several factors: chemical and physical perturbations, genetic changes, lack of its biological complementary molecules. Adaptative responses can contrast the chemical, physical and, to a lesser extent, genetic changes, but organisms can't restore by themselves a physiological condition, in the last situation.

For example, when the cell needs copper, it expresses the copper membrane uptaker. If extracellular copper availability is not enough, uptaker expression signal persistences and uptaker continues to be expressed. Otherwise, when extracellular copper is available uptaker is expressed untill cell no longer needs copper.

Prion protein is involved in copper uptake mechanism, as described above. Actually, it was demonstred that PrP^C binds cooperatively copper[6; 7; 8] and extracellular copper decreases PrP^C expression[148], but it also stimulates PrP^C endocytosis and cellular traffiking[36; 37; 38; 39]. Accordingly, it is resonable to think that PrP^C plays a primary role in copper homeostasis. An objection to this hypothesis is that it is known that copper transporter one (Ctr1) is the first copper channel[92]. An important feature of this transmembrane protein is that it is able to bind Cu^{1+}, while, in the extracellular medium, copper is present in the oxidized form[149]. This fact prevents that Ctr1 could bind copper directly. Since it was demonstred that PrP^C has high affinity for Cu^{2+} and

it was demontred that PrP^C reduces Cu^{2+} to Cu^{1+}, it is resonable to think that prion protein first binds copper ions and, after their reduction, Ctr1 can bind reduced copper ions and traslocates them into the cytoplasm.

When copper binds on octarepeats, it seems to promote also the α-helix structuring of this region[150]. Moreover, between two octarepeat triptophans there are seven aminoacids, that are two complete α-helix turns, so copper binding promotes also the stacking of triptophan indolic rings. So it is formed a zone that can allow hydrophobic interactions with other hydrophobic molecules, such as lipids or vitamins.

The theory developed by our research group proposes that prion protein plays a primary role in copper uptake. Moreover, PrP^C is endocytosed via endosome and lysosome pathway[21], so we think that copper uptake could happen via an endocytic pathway. Copper is an essential micronutrient (EMN). All EMNs share some important characteristics. Both metals and vitamins are present in micromolar concentrations, both in the body and foods. This feature can easily lead to deficiency. It is also clear that deficiency of EMNs produces overlapping diseases symptoms and for the reason that uptake of many vitamins happens via endocytic pathways[151; 152; 153; 154] and it is pH dependent, we hypothesize that prion protein and copper play a key role in common endocytic uptake pathway involving all EMNs.

Prion diseases can be explained because, when there is no intra and extracellular copper, prion protein is over expressed untill it reaches the solubility limit on the membrane surface, that causes the protein precipitation. PrP^C over expression is a *conditio sine qua non* to disease development[1]. If copper lack is lower and chronical, precipitation is slow, producing ordered aggregates (fibrils); otherwise, if copper lack is higher and acute, fast protein precipitation produces amorphous .

Toxic gain of function is commonly invoked to explain the phenotypes of other dominantly inherited neurodegenerative disorders, including Alzheimer's disease, Huntington's disease, Parkinson's disease and amyotrophic lateral sclerosis. In these disorders, it is postulated that intracellular or extracellular aggregates of the relevant

misfolded protein (Aβ, huntingtin, α- synuclein) possess a neurotoxic activity that is directly related to the normal, physiological function of the parent protein[155].

The aim of this work is to clarify if PrP^C allows micronutrients uptake.

To choose the experimental racombinant N-terminal peptide, we considered that PrP^C undergoes a variety of proteolytic processing events. In human brain, PrP^C is mainly endoproteolyzed on the N-terminal side, at the 110/111 peptidyl bond, to produce a 17 kDa C-terminal fragment (C1) tethered to the plasma membrane[156; 157]. A 9 kDa soluble N-terminal counterpart, referred to as N1, is released in the extracellular medium[158]. Little is known concerning the fact that these cleavages could be seen as an activating process leading to biologically active fragments or as an inactivating mechanism.

We first verified N-terminal domain interactions with five first transition serie divalent metals, checking binding parameters and structural protein changes at various pH values. Moreover, because *in vivo* metals are not free, but bound to various competitors, the same measures were repeated in presence of glycine, a weak metal ligand.

Another set of experiments were made up to check N-terminal domain interactions with four B group vitamins. In particular we chose vitamins with hydrophobic rings, that could be able to stack between triptophan indolic rings.

Finally, because PrP^C is localized on lipid raft domains, we checked if N-terminal domain interacts with membrane. To choose the membrane mimetic systems we considered that lipid raft domains are mainly characterized by a high content of sphingolipids and cholesterol. Furthermore, phosphatidylcholine, mainly with saturated acyl chains, is present, as well as small amounts of phosphatidylethanolamine and phosphatidylserine[159]. So we chose two membrane mimetic systems, one not charged and one negatively charged.

3. Metarials and Methods

3.1. Reagents

All used products are analytical grade reagents.

3.2. Protein expression

Professor Alessandro Negro supplied murine N-terminal prion protein ($mPrP^{23-109}$; Entrez nucleotide entry: M13685; UniProtKB/Swiss-Prot entry: P04925), cloned in pET-14b (figure 10).

Competent *E. coli*, BL21 (DE3) pLysS, were transformed with $mPrP^{23-109}$-pET14b plasmid, streaked on agar plate containing ampicillin (Amp) 100 μg/mL and incubated at 37°C overnight. After resuspension on plate, bacterial colonies were transferred in two flasks with one liter of Luria Bertani medium (LB), containing Amp 100 μg/mL, and growing at 37°C up to an optical density at 600 nm (OD_{600}) equal to 0.6. Induction was carried out with IPTG 100 mg/L, at 37°C for 4 hours.

Colture broth was centrifuged at 2000 g for 15 minutes at 4°C. Once discarded supernatant, pellets were resuspended in PBS (NaCl 140 mM, KCl 2.7 mM, K/phosphate buffer 10 mM, pH 8.0) and stored at -20°C until purification.

Expression goodness was tested with a SDS-PAGE.

3.3. Protein purification

To destroy cell membranes and inclusion bodies, bacterial suspensions were sonicated (LABSONIC U, B. BRAUN) adding small aliquots of Denaturing Solution (guanidinium chloride 6 M, K/phosphate buffer 100 mM, Tris 10 mM, pH 8.0).

After sonication, samples were centrifuged at 15000 g, for 30 minutes at 4°C and supernatants were collected.

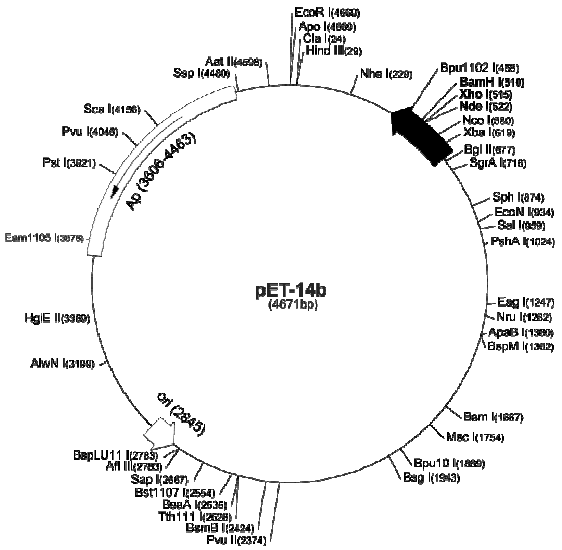

Figure 10: pEt-14b plasmid map.

These were added to 3 ml of equilibrated His-tag affinity resin (Ni-NTA Agarose, purchased by Qiagen) and were stirred for one hour. Thanks to the six histidines tagged to $mPrP^{23\text{-}109}$, it binds to resin nickel ions, at basic pH.

Non bound proteins were washed out with 20 volumes of denaturing solution and 20 volumes of Urea Buffer (urea 8 M, K/phosphate buffer 100 mM, Tris 10 mM, pH 8.0).

Bound proteins were eluted with Urea Buffer, pH 5.9. All fraction concentrations were analyzed with a UV/visible spectrophotometer (Hewlett Packard, diode spectrophotometer, 8452A) using the Lambert-Beer law:

$$Abs_{280} = \varepsilon \times c \times l$$

in which Abs_{280} is the measured absorbance at 280 nm, ε is extinction molar coefficient, c is protein concentration and l is the optical path expressed in centimetres. Theoretical extinction molar coefficient was calculated with ExPASy ProtParam tool and it results 41480 $M^{-1}cm^{-1}$.

Fractions with higher concentration were combined.

To change buffer solution, eluate was dialyzed with a 3500 molecular weight cut off membrane tube (MWCO), purchased by Spectra/Por, versus Storing Buffer (Na/acetate buffer 50 mM, pH 4.5).
Finally, samples were stored at -20°C, in presence of sucrose 20% (p/v).

3.4. His-tag cut

3.4.1. Theoretical principles

To cut His-tag I used thrombin from human plasma, purchased by Sigma-Aldrich (product number T6884).
Thrombin is an enzyme that recognizes and cuts two amino acid sequences. First one is:

A-B-Pro-Arg-||-X-Y

where A and B are hydrophobic amino acids and X and Y are non acidic amino acids. Second cleavage site is:

Gly-Arg-||-Gly^{160}

Thrombin is active in the pH range of 5-10 and it precipitates at pH 5 or less. Its "catalysis optimum" pH is 8.3 and concentration is 0.5 units thrombin per one nanomole polypeptide.
Two protocols were developed.

3.4.2. Dialysis protocol

To change Storing Buffer in the Thrombin Buffer (Tris 50 mM pH 8.3, NaCl 150 mM, $MgCl_2$ 2.5 mM), an aliquot of protein solution was dialyzed using a 3500 MWCO membrane tube (Spectra/Por) versus thrombin buffer, at 4°C.

Then, an aliquot of thrombin was added, obtaining the optimum ratio thrombin/polypeptide. Reaction was performed overnight at room temperature.
At the end of the cutting reaction, buffer was changed in the storing one, as described above.
Finally, protein concentration was measured as described in §3.3.

3.4.3. Precipitation protocol

Four volumes of acetone, cooled at -20°C, were added to an aliquot of protein, in Storing Buffer, and this solution was stored at -20°C for 3 hours. This procedure precipitates all protein so, after that, samples were centrifuged at 18000 g, for 40 minutes at 4°C. Supernatant was discarded and samples were totally dried in a SPEED VAC, SC110 Savant.
Then samples were resuspended in an appropriate volume of Thrombin Buffer and an aliquot of thrombin was added. Reaction was performed overnight at room temperature.
At the end of the cutting reaction, buffer was changed in the Storing Buffer, using the same procedure.
Finally, protein concentration was measured as described in §3.3 and expression goodness was tested in a SDS-PAGE.

3.5. SDS-PAGE

All purification steps were analyzed by 16% SDS-PAGE. Gel compositions are listed in table 2.
To each sample was added a Sample Buffer (Tris 50 mM pH 8.9, urea 8 M, SDS 1%, dithiothreitol (DTT) 1mM, monoiodoacetamide (MIA) 2 mM, glycerol 20%) and mixtures were incubated for two hours before loading.
Samples were run at 4°C at 20 mA per gel using a Mini-Protean 3 cell, purchased by BIORAD. Proteins were visualized by Blue Coomassie staining (Brilliant Blue Coomassie 0.1%, methanol 5/11, acetic acid 1/11 and milliRo water 5/11).

Stock solutions	Resolving gel (16%)	Stacking gel (5%)
Acrylamide 40%	4.000	**0.625**
Bisacrylamide 1.6%	3.125	**0.488**
Tris 3 M pH 8.9	1.667	**/**
Tris 0.5 M pH 6.8	/	**1.250**
SDS 10%	0.100	**0.050**
APS 10%	0.070	**0.035**
TEMED	0.007	**0.004**
H_2O	1.030	**2.548**
Total volume (ml)	**10.000**	**5.000**

Table 2: Composition of stacking and resolving gels. All volume values are expressed in millilitres. Ratio acrylamide/bisacrylamide is 48.0/1.5.

Low molecular weight range markers (table 3), purchased by Sigma (M3913), were used to estimate the recombinant proteins molecular weight.

Protein	Molecular Weight (Da)
Albumin (bovine serum)	**66.000**
Ovalbumine (chicken egg)	**45.000**
Glyceraldehyde 3-P Dehydrogenase (rabbit muscle)	**36.000**
Carbonic Anhydrase (bovine erythrocytes)	**29.000**
Trypsinogen (bovine pancreas)	**24.000**
Trypsin Inhibitor (soybean)	**20.000**
α-Lactalbumin (bovine milk)	**14.200**
Aprotinin (bovine lung)	**6.500**

Table 3: Protein composition of Low Molecular Weight Range Markers (M3913, Sigma).

3.6. Mass spectrometry

For electrospray ionization mass spectrometry analysis the protein was resuspended in 10 μL of solution, composed by 49% H_2O mQ, 50% acetonitrile and 1% formic acid. Analysis was made in collaboration with Dr. P. James (Biomedical center of Lund University).

3.7. Solubility measurements

To know protein solubility at pH 7.4, somes aliquots of $mPrP^{23-109}$ were concentrated six times using 3000 MWCO polyethersulfone concentrators (Vivaspin 500). Every concentration step was followed by a concentration measurement (§3.3).

3.8. Atomic absorption measurements

To know if there were metals contaminations in used solutions, atomic absorption measurements were recorded on a Perkin Elmer AAnalyst 100 instrument. Table 4 shows measurement parameters.

Metals	Wavelength (nm)	Slit (nm)	Flame gases	Standard conc (ppm)
Cobalt (Co)	240.7	0.2	Air/Acetilene	7.0
Copper (Cu)	324.8	0.7	Air/Acetilene	4.0
Iron (Fe)	248.3	0.2	Air/Acetilene	5.0
Manganese (Mn)	279.5	0.2	Air/Acetilene	2.5
Nickel (Ni)	232.0	0.2	Air/Acetilene	7.0
Zinc (Zn)	360.1	0.2	Air/Acetilene	1.0

Table 4: Atomic absorption measurement parameters. Standard solution concentrations are expressed in part per million (ppm).

3.9. Metal binding parameters analysis

3.9.1. Theoretical principles in fluorescence spectroscopy

A molecule can possesses only discrete amounts of energy. The potential energy levels of the molecule are described by an energy level diagram (figure 11).

This figure shows two electronic levels, the ground state (G) and the first exited state (S_1) and some of the vibrational levels of each. Light energy can be absorbed only when the molecule moves from a lower to a higher energy level. If the molecule is initially unexcited (G) and the absorbed energy is greater than required to reach S_1,

the excess energy is absorbed as vibrational energy. This vibrational energy is rapidly dissipated as heat by collision with solvent molecules, and the molecule drops to the lowest vibrational level of S_1. the excited molecule then returns to G by emitting light (fluorescence) or by a non-radiative transition.

Because energy is lost in dropping to the lowest level of S_1, the emitted light will have less energy (longer wavelength) than the absorbed light. However, in returning to G, the molecule may arrive at one of the vibrational levels of G, dissipating remaining energy as heat. Hence, if there are many absorbers, the light emitted will have many wavelengths and the probability of dropping from S_1 to each vibrational level of G determines the shape of the fluorescence spectrum.

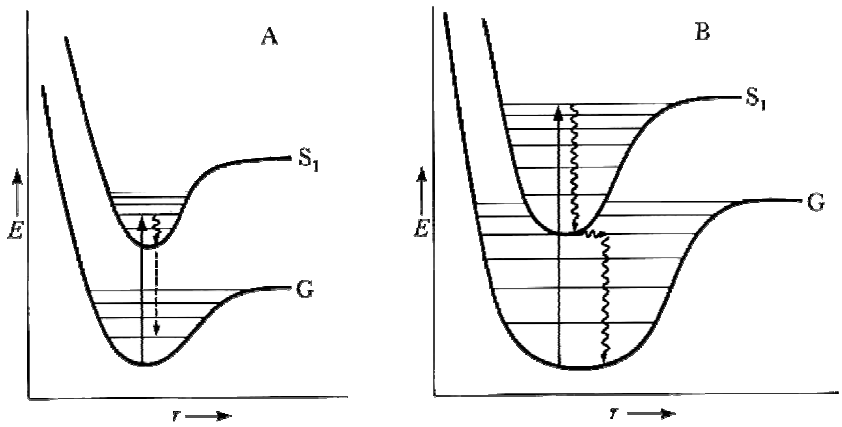

Figure 11: Energy level diagram of two chromophores. G and S_1 indicate the ground and the first excited states, respectevely. The vibrational levels are the thin lines. In panel A is showing a molecule capable of fluorescing. After excitation, there are vibrational losses (wavy arrow) to the lowest level of S_1 and then emission from this state (dashed arrow). In panel B is showing a molecule that fails to fluorescence because the vibrational levels of G are higher than the lowest level of S_1. Hence, there can be a non radiative transition (horizontal wavy arrow) followed by non radiative energy losses to the bottom of G.

3.9.2. Metal titrations in fluorescence spectroscopy

To know $mPrP^{23-109}$ metals binding dissociation constants and cooperativity binding grade, $mPrP^{23-109}$ was titrated with metal salts (listed in table 5) at five different pH (pH buffers are listed in table 6).

Metal Salt	Formula	Stock concentration
Copper acetate	$(CH_3COO)_2Cu*H_2O$	100 mM
Nickel sulphate	$NiSO_4*6H_2O$	100 mM
Manganese chloride	$MnCl_2*4H_2O$	100 mM
Zinc sulphate	$ZnSO_4*7H_2O$	100 mM
Cobalt chloride	$CoCl_2*6H_2O$	100 mM

Table 5: Metal salts used in $mPrP^{23-109}$ titration.

Buffer	Concentration	pH
Na/acetate	50 mM	4.0
Na/acetate	50 mM	5.0
Na/acetate	50 mM	6.2
NEM	50 mM	7.4
NEM	50 mM	8.6

Table 6: Fluorescence buffers. These buffers were chosen because they do not interact with metals[161].

Measures were made using a quartz cuvette with 1 cm optical path in a Perkin Elmer fluorimeter (LS50). Table 7 shows working parameters.

Moreover, because *in vivo* metals are not free, but bound to various competitors, the same measures described above were repeated in presence of glycine 1 mM.

Instrument setup	
Start wavelength	300 nm
End wavelength	450 nm
Excitation wavelength	295 nm
Scan speed	240 nm/min
Emission slit	Variable
Excitation slit	Variable
Accumulation	4
Temperature	35°C

Table 7: Operating fluorimeter parameters.

Data were fitted after doing some considerations. First consideration is that two types of metal atom quench fluorophore fluorescence: bound and unbound atoms. So total quenching is described by the following formula:

$$Q_t = Q_b + Q_s$$

in which Q_t is total quenching, Q_b is quenching due to bound metals, Q_s is quenching due to unbound metals. Similarly, quenching function is:

$$F_{xt} = F_{xb} + F_{xs}$$

Unbound metal quenching follows a linear function, so F_{xs} is:

$$F_{xs} = s \times x$$

where x is metal concentration and s is the slope.
Because prion protein is a cooperative system, F_{xb} follow the Hill equation:

$$Y = \frac{x^n}{K_d + x^n}$$

where Y is the saturation fraction, x is the metal concentration, n is the Hill number and K_d is the dissociation constant. Hill number is an important index that identifies the binding domain interaction degree; if it is more than one cooperation is positive, if it is less cooperation is negative. It also should be noted that in ideal quenching,

schematized in figure 12, saturation fraction is also described by the following equation:

$$Y = \frac{F_0 - F_x}{F_0 - F_f}$$

where F_0 is initial fluorescence without metal, F_x is fluorescence during metal titration and F_f is saturated system fluorescence.

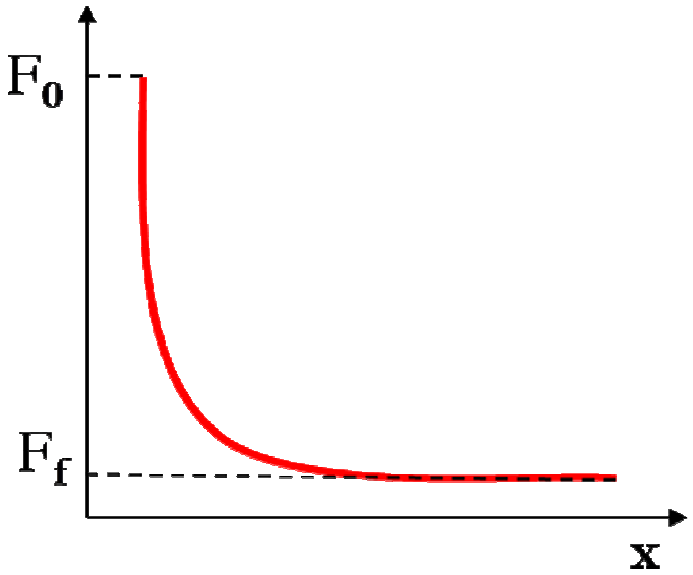

Figure 12: Ideal quenching sheme.

Combining all previous formulae, the following final formula was obtained:

$$F_{xb} = s \times x - \frac{x^n \times (F_0 - F_f)}{K_d + x^n} + F_0$$

This formula describes bound metal quenching as function of metal concentration. Data were fitted using OriginPro 8.0.

3.10. Metal structural analysis

3.10.1. Theoretical principles of circular dichroism

When a beam of light passes through the matter, the electric vector of the propagating wave interacts with the electrons of the component atoms. This interaction has the effect of reducing the velocity of propagation (refraction) and in decreasing the amplitude of the vector (absorption). These two effects are described by the index of refraction, n, and the molar absorption coefficient, ε. When a molecule is sensitive to the plane of polarization of the incident light, it is optically active and it is characterized by having distinct indices of refraction (n_L, n_R) and molar absorption coefficients (ε_L, ε_R) for left and right circularly polarized light. Optical activity is proper of chiral molecules. So if a beam of circularly polarized light passes trough a optical active matter, in range of wavelengths in which absorption occurs, there will be differential absorption of the L and R polarize light. This difference (ε_L-ε_R) is the circular dichroism (CD).

3.10.2. Metal titrations in circular dichroism

To know mPrP$^{23\text{-}109}$-metals structural binding characteristics, mPrP$^{23\text{-}109}$ was titrated with metal salts (table 5), using three different pH, showed in table 6 (pH 7.4, 6.2, 5.0), at a concentration of 10 mM.

Measures were made using a quartz cuvette with 0.2 cm optical path in a Jasco J-810 spectropolarimeter. Table 8 shows working parameters.

To determine if metal binding induces conformational changing and, hence, if metal binding is functional, data were analyzed in the following manner. In each CD graph were taken values at 222 nm (a) and 198 nm (b) as, respectively, α-helix and random coiled structure indices. These were used to build a third index (S), as show the following formula:

$$S = \frac{a}{b}$$

If adding metal salt *S* increases, it means that the metal induces structuring of protein; on the contrary, if *S* decreases, the metal induces destructuring of protein.

Instrument setup	
Sensitivity	100 mdeg
Start	250 nm
End	190 nm
Data pitch	0.1 nm
Scan speed	50 nm/min
Band width	10
Response	2 sec
Accumulation	4
Temperature	room

Table 8: Operating fluorimeter parameters.

3.11. Vitamin binding analysis

3.11.1. Theoretical principles of fluorescence anisotropy

When a beam of linear polarized light passes through the matter containing a fluorophore, it preferentially excites molecules with transition dipole moment parallel to electric field direction vector. If fluorophore motion speed is low, fluorescence will be polarized too; on the other hand, if it is high and it can collide with other molecules before light emission, fluorescence will be depolarized. So fluorescence anisotropy measurements can investigate molecular motion speed.

Anisotropy (*A*) is defined by the following equation:

$$A = \frac{I_{//} - I_{\perp}}{I_{//} + 2I_{\perp}}$$

in which, $I_{//}$ and $I_{\perp}$ are fluorescence intensity when emission polarizator is parallel or perpendicular, respectively, to the excitation polarizator.

3.11.2. Vitamin titration in fluorescence anisotropy

To know if vitamins interact with mPrP$^{23\text{-}109}$, tryptophan anisotropy was measured during vitamin titrations, in presence of copper acetate 80 mM, at pH 7.4 (table 6). Used vitamins are listed in table 9.

Vitamin	Stock concentration
Thiamine hydrochloride	100 mM
Riboflavin (-)	100 mM
Nicotinamide	100 mM
Pyridoxine hydrochloride	100 mM

Table 9: Vitamins used in mPrP$^{23\text{-}109}$ titration.

Measures were made using a quartz cuvette with 1 cm optical path in a Perkin Elmer fluorimeter (LS50). Table 10 shows working parameters.

Instrument setup	
Excitation wavelength	295 nm
Emission wavelength	354 nm
Emission slit	10
Excitation slit	10
Integration time	1.00 sec
Accumulations	30
Temperature	35°C

Table 10: Operating anisotropy parameters.

3.12. Large unilamellar vesicles (LUVs) interaction

3.12.1. LUVs preparation

3.12.1.1. Injection

To avoid light scattering, vesicle diameter has to be less than 200 nm.

Dimyristoyl-phosphatidyl-choline (DMPC), purchased by Sigma (P2663), were dissolved in absolute ethanol, reaching the concentration of 50 mM. This solution was very slowly injected in a stirred solution of N-etylmorpholine (NEM) buffer 1 mM, pH 7.4, 35°C[162], reaching final phospholipid concentration of 8 mM.

3.12.1.2. Extrusion

In this protocol was used the Mini-Extruder (Avanti Polar Lipids).

An amount of dioleoyl-phosphatidyl-glycerol (DOPG), purchased by Sigma (P9664), was totally evaporated with a constant nitrogen flux, leaving a thin lipid film on vial bottom. Lipids were hydrated adding NEM buffer 1 mM, pH 7.4, to reach final phospholipid concentration of 8 mM, and vortexing to dissolve lipid film.

This solution was inserted in a syringe and the extruder was assembled using extrusion membrane with a 50-100 nm cut off, purchased by Millipore. To obtain a homogenous lipid solution, this passed through the membrane at least 50 times.

3.12.2. LUVs imaging: electron microscopy

Transmission Electron microscopy was performed on negatively stained samples, using a transmission electron microscope (TEM) FEI Tecnai G2. Uranyl acetate 1% was added to 350 μM phospholipid solutions. All pictures were recorded in collaboration with Mr. G. Tognon (C.N.R.).

3.12.3. LUVs titration in fluorescence spectroscopy

To know if $mPrP^{23-109}$ interacts with neutral or negatively charged LUVs, it was titrated with LUV stock solutions (prepared as described in §3.12.1.1 and §3.12.1.2) at three different pH, 5.0, 6.2, 7.4 (table 6) and in presence of copper 80 μM.

Measures were made using a quartz cuvette with 1 cm optical path in a Perkin Elmer fluorimeter (LS50). Table 11 shows working parameters.

Instrument setup	
Start wavelength	310 nm
End wavelength	400 nm
Excitation wavelength	295 nm
Scan speed	240 nm/min
Emission slit	Variable
Excitation slit	Variable
Accumulation	4
Temperature	35°C

Table 11: Operating fluorimeter parameters.

4. Results

4.1. Expression and purification

SDS-PAGE analysis was used to test goodness of protein expression, purification and His-tag cutting.

Figure 13 shows cellular extracts of *E. coli* transformed with PrP23-109 cloned pET-14b (lanes *a*, *b* and *c*), compared with the same cell line transformed with empty vector (lane *d*).

Prion protein was then purified as indicated in §3.3. All undesired proteins were eliminated in a one step affinity cromatography, as results in the lane *f* of figure 13. After purification, protein concentration was about 70 μM, in store buffer.

His-tag was eliminated as indicated in §3.4.3 and result is showed in lane *h* of figure 13. After thrombin treatment, protein was diluted in store buffer, restoring the previous concentration (70 μM).

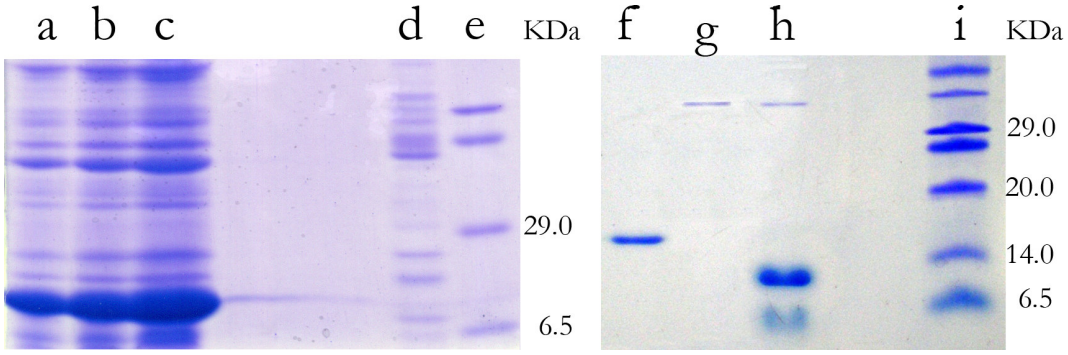

Figure 13: SDS-PAGE analysis. In lanes *a*, *b* and *c* there are three different concentration lysates of *E. coli* transformed with PrP^{23-109} cloned pET-14b; in lane *d* there is the same cell line transformed with empty pET-14b. In lane *f* there is the His-tag affinity chromatography elution result; in lane *h* there is the Thrombin cutting protocol result; in lane *g* there is the Thrombin cutting result without eluted protein. In lanes *e* and *i* there are two different SDS-PAGE markers.

Figure 14 shows the final purified peptide sequence compared with the deposited sequence P04925, using EBI ClustalW tool. Recombinant sequence molecular weight is 9154.8 Da and its theoretical isoelectri point is 11.26 (ExPASy ProtParam tool). Table 12 shows aminoacid composition.

```
recombinant       --------------------GSKKRPKPGGWNTGGSRYPGQGSPGGNRYPPQGGTWGQPH 40
P04925            MANLGYWLLALFVTMWTDVGLCKKRPKPGGWNTGGSRYPGQGSPGGNRYPPQGGTWGQPH 60
                                      .************************************

recombinant       GGGWGQPHGGSWGQPHGGSWGQPHGGGWGQGGGTHNQWNKPSKPKTNLK----------- 89
P04925            GGGWGQPHGGSWGQPHGGSWGQPHGGGWGQGGGTHNQWNKPSKPKTNLKHVAGAAAAGAV 120
                  ************************************************

recombinant       ------------------------------------------------------------
P04925            VGGLGGYMLGSAMSRPMIHFGNDWEDRYYRENMYRYPNQVYYRPVDQYSNQNNFVHDCVN 180

recombinant       ------------------------------------------------------------
P04925            ITIKQHTVTTTTKGENFTETDVKMMERVVEQMCVTQYQKESQAYYDGRRSSSTVLFSSPP 240

recombinant       --------------
P04925            VILLISFLIFLIVG 254
```

Figure 14: Alignment of sequenced recombinant mPrP$^{23\text{-}109}$ with the deposited sequence P04925.

Aminoacid	Abbreviation	Number	Percentage (%)
Arg	R	3	3.4
Asn	N	5	5.6
Gln	Q	8	9.0
Gly	G	29	32.6
His	H	5	5.6
Leu	L	1	1.1
Lys	K	7	7.9
Pro	P	12	13.5
Ser	S	6	6.7
Thr	T	4	4.5
Trp	W	7	7.9
Tyr	Y	2	2.2
total		89	100

Table 12: Aminoacid composition of the expressed and purified peptide.

Finally, figure 15 shows multi charge ESI spectrum of the purified N-terminal domain.

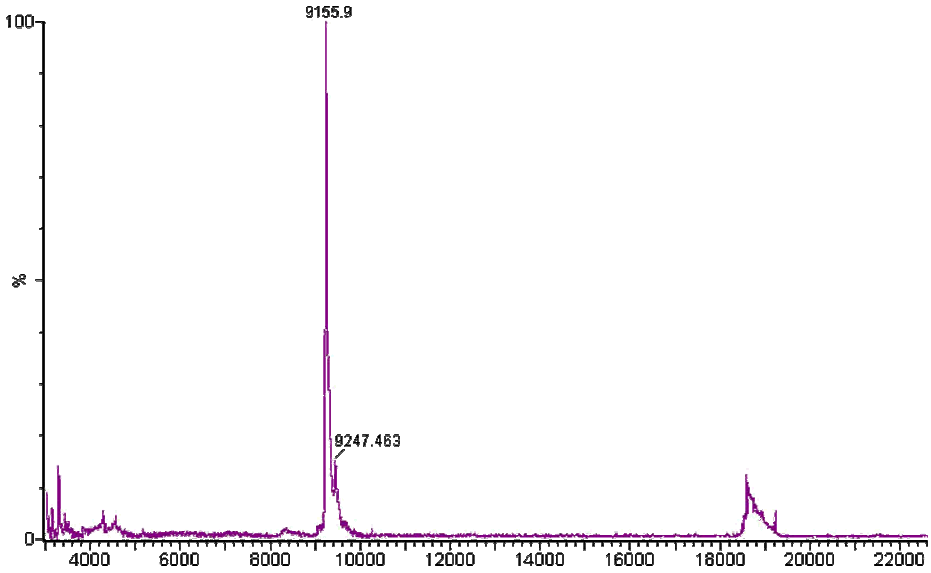

Figure 15: ESI spectrum of the purified N-terminal domain.

4.2. Solubility

Prion protein N-terminal domain solubility at pH 7.4 was checked as described in §3.7. Figure 16 shows that this domain is soluble at least until about 250 μM.

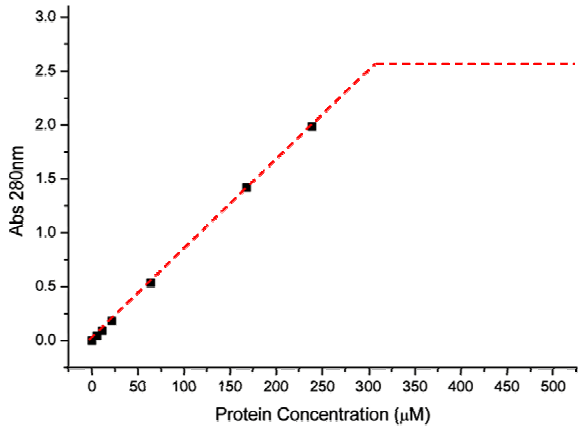

Figure 16: Absorbance at 280 nm in function of protein concentration. Dotted line is the theoretical solubility curve and square points are experimental data of $mPrP^{23-109}$ concentrated in NEM 50 mM, pH 7.4.

4.3. Metals PrP$^{23-109}$ binding

4.3.1. Binding parameters analysis

Fluorescence titrations were made as described in §3.9.2.

Figures 17 to 21 show experimental data and fitting curves of mPrP$^{23-109}$ titrated at different pH values with copper acetate, nickel sulfate, zinc sulfate, manganese chloride and cobalt chloride, respectevely.

Table 13 shows, for each metal and pH, dissociation constant values (K_d).

Table 14 shows, for each metal and pH, Hill number (n) and the relative standard deviation.

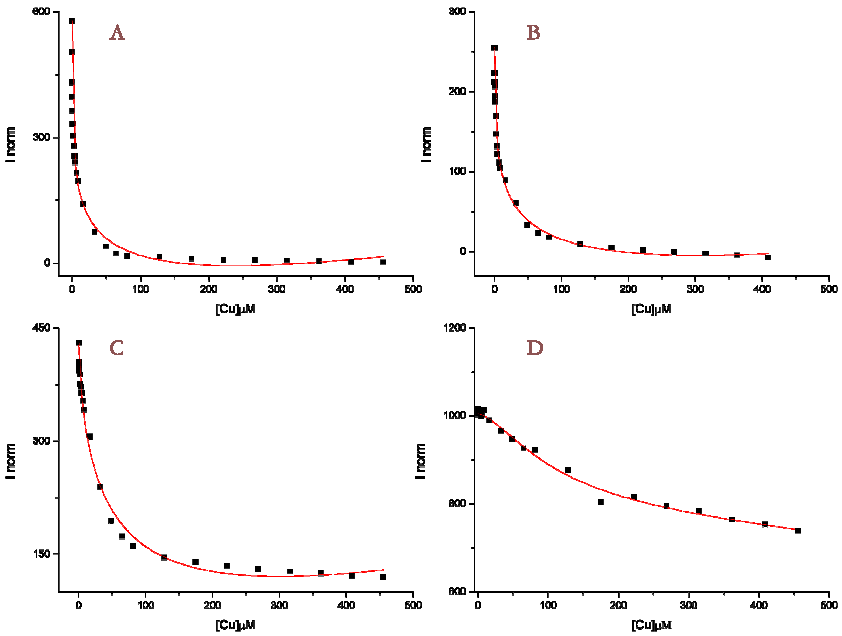

Figure 17: Normalized mPrP$^{23-109}$ fluorescence values (*I norm*) versus copper concentration at different pH values. Panel A is at pH 8.6; Panel B is at pH 7.4; Panel C is at pH 6.2; Panel D is at pH 5.0.

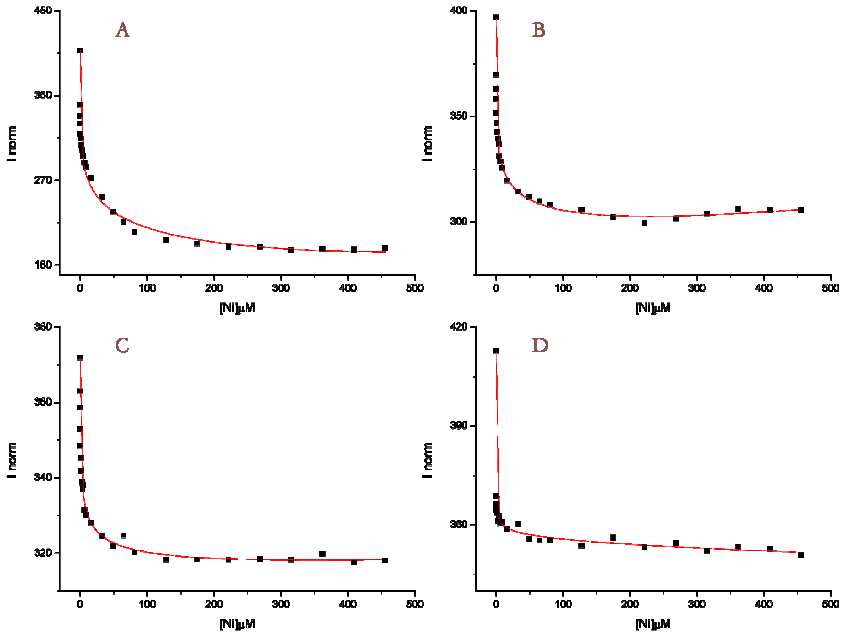

Figure 18: Normalized mPrP$^{23\text{-}109}$ fluorescence values (*I norm*) versus nickel concentration at different pH values. Panel A is at pH 8.6; Panel B is at pH 7.4; Panel C is at pH 6.2; Panel D is at pH 5.0.

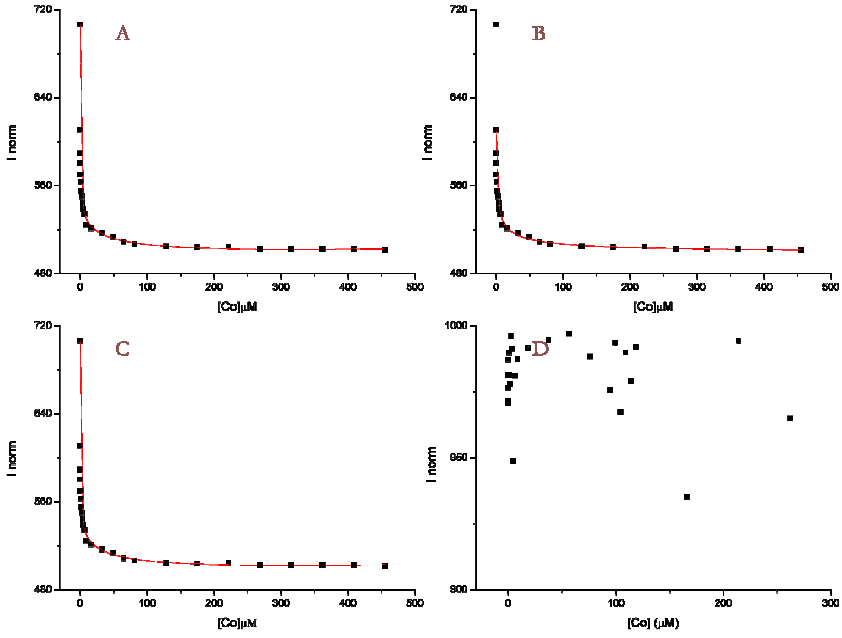

Figure 19: Normalized mPrP$^{23\text{-}109}$ fluorescence values (*I norm*) versus cobalt concentration at different pH values. Panel A is at pH 8.6; Panel B is at pH 7.4; Panel C is at pH 6.2; Panel D is at pH 5.0.

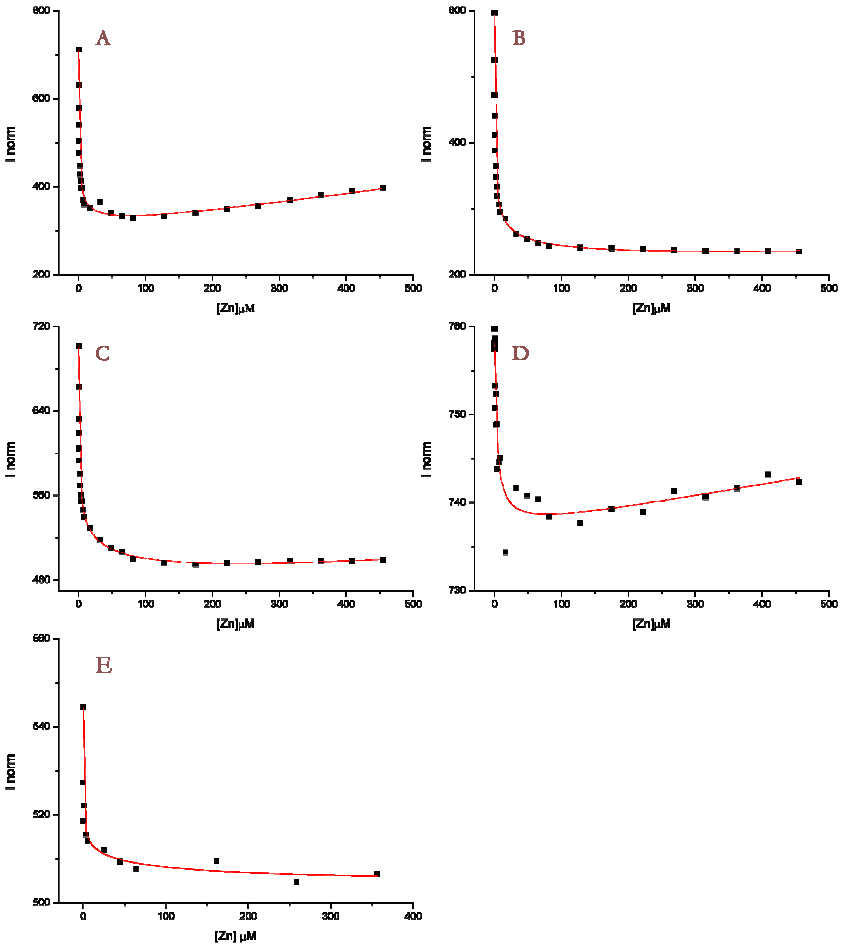

Figure 20: Normalized mPrP$^{23\text{-}109}$ fluorescence values (*I norm*) versus zinc concentration at different pH values. Panel A is at pH 8.6; Panel B is at pH 7.4; Panel C is at pH 6.2; Panel D is at pH 5.0; Panel E is at pH 4.0.

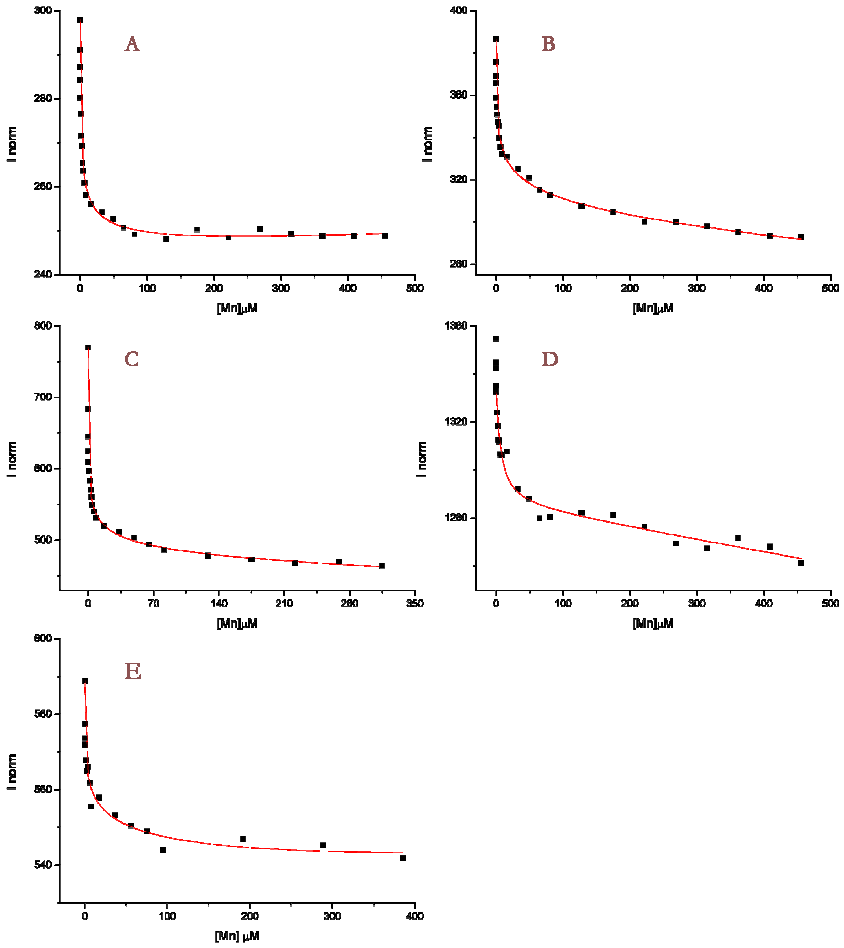

Figure 21: Normalized mPrP$^{23\text{-}109}$ fluorescence values (*I norm*) versus manganese concentration at different pH values. Panel A is at pH 8.6; Panel B is at pH 7.4; Panel C is at pH 6.2; Panel D is at pH 5.0; Panel E is at pH 4.0.

pH	Copper	Nickel	Zinc	Manganese	Cobalt
8.6	10^{-6} M	10^{-2} M	10^{-6} M	10^{-6} M	10^{-6} M
7.4	10^{-6} M	10^{-6} M	10^{-6} M	10^{-6} M	10^{-6} M
6.2	10^{-5} M	10^{-6} M	10^{-6} M	10^{-6} M	10^{-6} M
5.0	10^{-3} M	10^{-4} M	10^{-6} M	10^{-5} M	nd
4.0	nd	nd	10^{-6} M	10^{-6} M	nd

Table 13: Dissociation constant (K_d) values relative to mPrP$^{23\text{-}109}$ metals binding, at different pHs.

pH	Copper	Nickel	Zinc	Manganese	Cobalt
8.6	0.30±0.03	0.16±0.05	0.46±0.04	0.49±0.03	0.23±0.03
7.4	0.37±0.03	0.21±0.02	0.42±0.03	0.33±0.03	0.53±0.28
6.2	0.68±0.09	0.39±0.04	0.34±0.03	0.30±0.04	0.23±0.03
5.0	1.63±0.44	0.03±0.00	0.89±0.24	1.14±0.48	nd
4.0	nd	nd	0.18±0.17	0.24±0.09	nd

Table 14: Hill numbers resulting in titrations done in absence of glycine. It is indicated standard deviation and *nd* means not determined.

Figures 22 to 25 show experimental data and fitting curves of $mPrP^{23\text{-}109}$ titrated at different pH values with copper acetate, nickel sulfate, zinc sulfate, manganese chloride and cobalt chloride, respectevely, in presence of glycine 1 mM.

Table 15 shows, for each metal and pH, dissociation constant values (K_d).

Table 16 shows, for each metal and pH, Hill number (n) and the relative standard deviation.

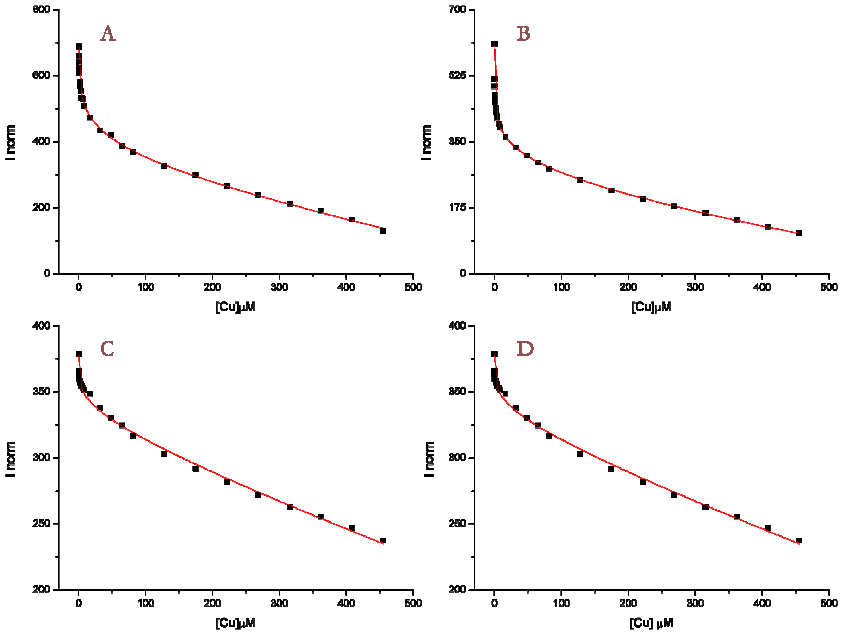

Figure 22: Normalized $mPrP^{23\text{-}109}$ fluorescence values (*I norm*) versus copper concentration in presence of glycine 1 mM, at different pH values. Panel A is at pH 8.6; Panel B is at pH 7.4; Panel C is at pH 6.2; Panel D is at pH 5.0.

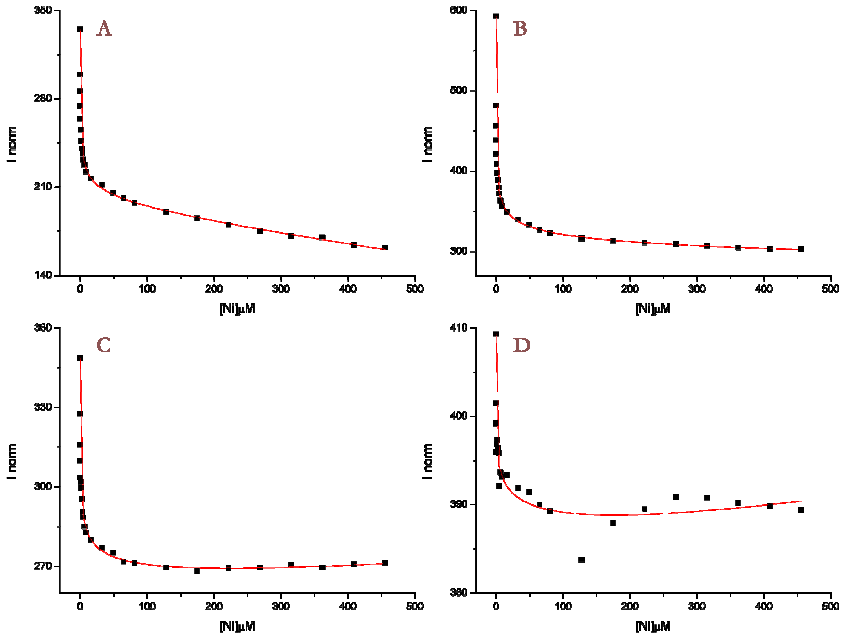

Figure 23: Normalized mPrP$^{23\text{-}109}$ fluorescence values (*I norm*) versus nickel concentration in presence of glycine 1 mM, at different pH values. Panel A is at pH 8.6; Panel B is at pH 7.4; Panel C is at pH 6.2; Panel D is at pH 5.0.

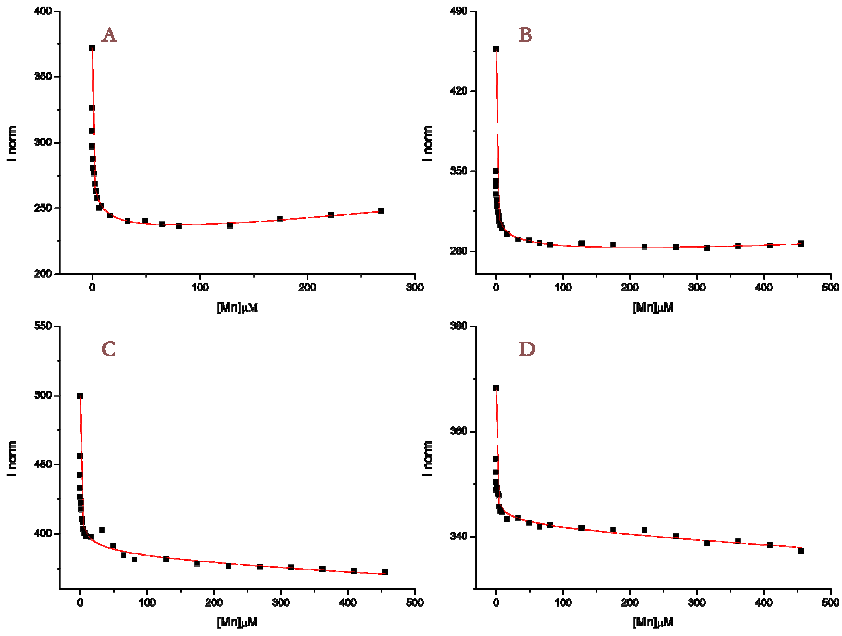

Figure 24: Normalized mPrP$^{23\text{-}109}$ fluorescence values (*I norm*) versus manganese concentration in presence of glycine 1 mM, at different pH values. Panel A is at pH 8.6; Panel B is at pH 7.4; Panel C is at pH 6.2; Panel D is at pH 5.0.

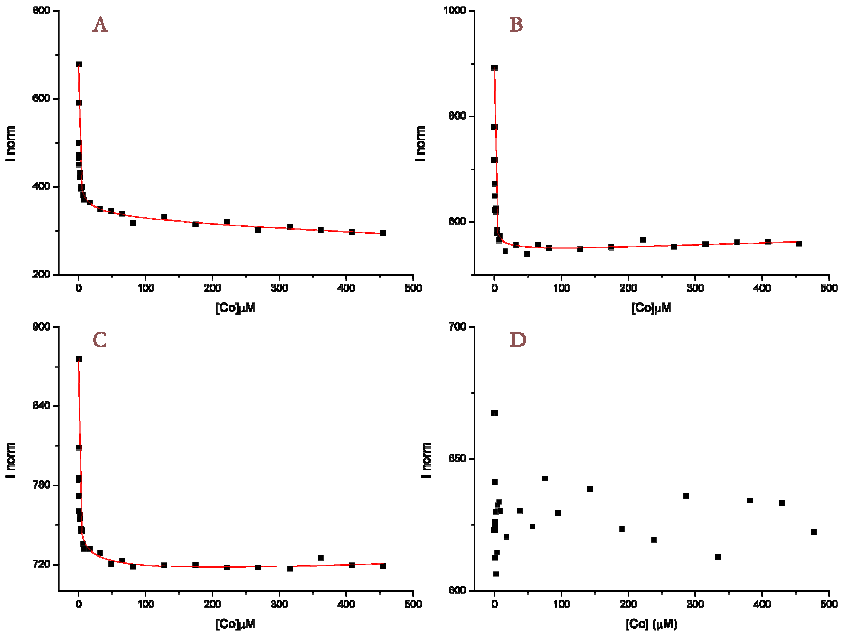

Figure 25: Normalized mPrP$^{23-109}$ fluorescence values (*I norm*) versus cobalt concentration in presence of glycine 1 mM, at different pH values. Panel A is at pH 8.6; Panel B is at pH 7.4; Panel C is at pH 6.2; Panel D is at pH 5.0.

pH	Copper	Nickel	Manganese	Cobalt
8.6	10^{-6} M	10^{-6} M	10^{-6} M	10^{-6} M
7.4	10^{-3} M	10^{-6} M	10^{-6} M	10^{-7} M
6.2	10^{-2} M	10^{-6} M	10^{-6} M	10^{-6} M
5.0	10^{-2} M	10^{-3} M	10^{-6} M	nd

Table 15: Dissociation constant (K_d) values relative to mPrP$^{23-109}$ metals binding in presence of glycine 1 mM, at different pHs.

pH	Copper	Nickel	Manganese	Cobalt
8.6	0.36±0.03	0.36±0.02	0.32±0.04	0.38±0.06
7.4	0.15±0.02	0.27±0.02	0.14±0.02	0.52±0.07
6.2	0.20±0.09	0.29±0.00	0.31±0.05	0.28±0.04
5.0	0.20±0.09	0.12±0.12	0.21±0.07	nd

Table 16: Hill numbers resulting in titrations done in presence of glycine 1 mM. It is indicated standard deviation and nd means not determined.

4.3.2. Structural analysis

Circular dichroism measures were made as described in §3.10.2.

Figures 26 to 30 show experimental CD graphs of $mPrP^{23-109}$ titrated at different pH values with copper acetate, nickel sulfate, zinc sulfate, manganese chloride and cobalt chloride, respectevely.

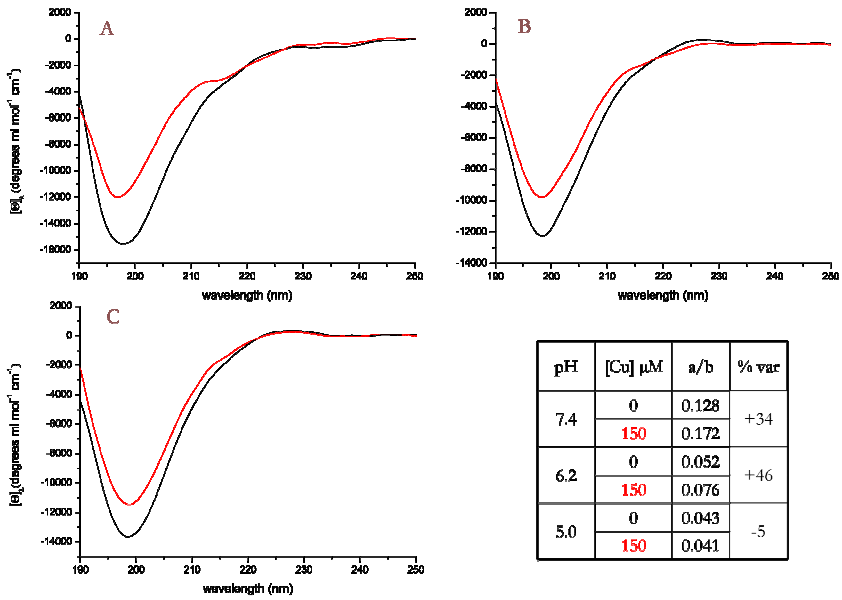

pH	[Cu] µM	a/b	% var
7.4	0	0.128	+34
	150	0.172	
6.2	0	0.052	+46
	150	0.076	
5.0	0	0.043	-5
	150	0.041	

Figure 26: Circular dicroism spectra at different pH values (panel A is at pH 7.4; panel B is at pH 6.2; panel C is at pH 5.0). Black lines are in absence and red ones are in presence of copper acetate 150 mM. In table are reported the structuring index (*a/b*) and the percentage of variance (*% var*).

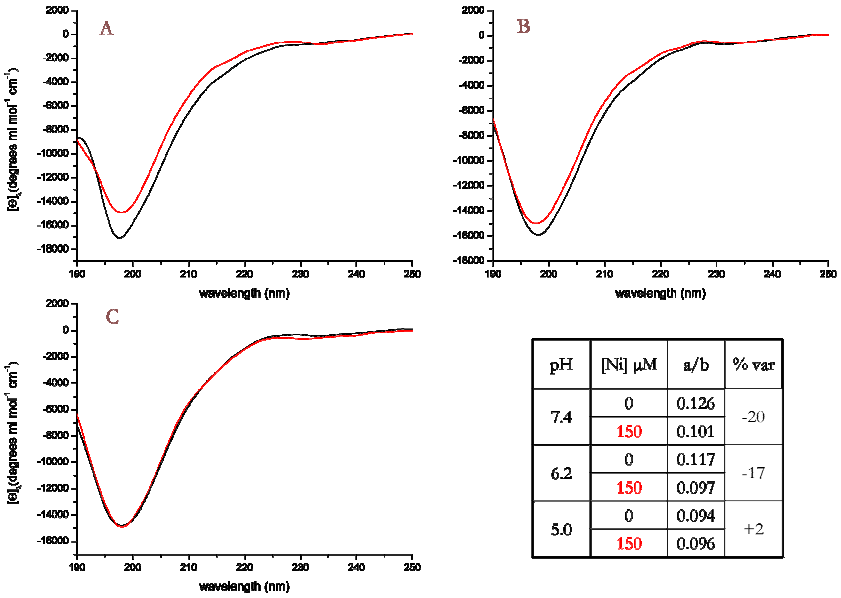

pH	[Ni] µM	a/b	% var
7.4	0	0.126	-20
	150	0.101	
6.2	0	0.117	-17
	150	0.097	
5.0	0	0.094	+2
	150	0.096	

Figure 27: Circular dicroism spectra at different pH values (panel A is at pH 7.4; panel B is at pH 6.2; panel C is at pH 5.0). Black lines are in absence and red ones are in presence of nickel sulfate 150 mM. In table are reported the structuring index (*a/b*) and the percentage of variance (*% var*).

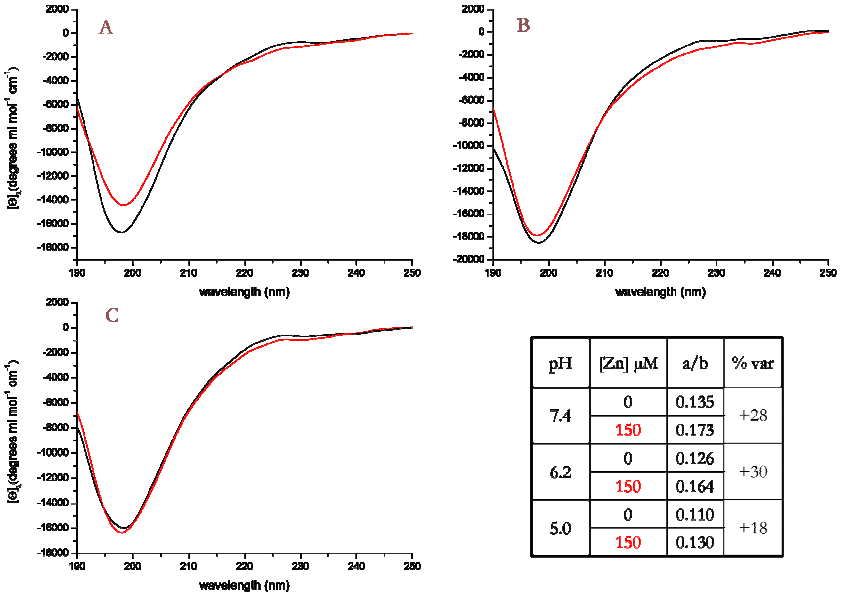

pH	[Zn] µM	a/b	% var
7.4	0	0.135	+28
	150	0.173	
6.2	0	0.126	+30
	150	0.164	
5.0	0	0.110	+18
	150	0.130	

Figure 28: Circular dicroism spectra at different pH values (panel A is at pH 7.4; panel B is at pH 6.2; panel C is at pH 5.0). Black lines are in absence and red ones are in presence of zinc sulfate 150 mM. In table are reported the structuring index (*a/b*) and the percentage of variance (*% var*).

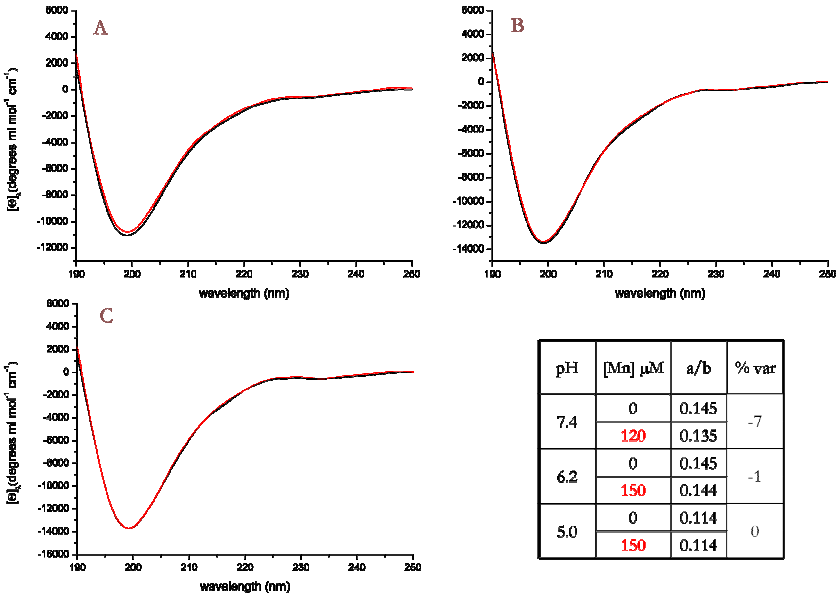

pH	[Mn] μM	a/b	% var
7.4	0	0.145	-7
	120	0.135	
6.2	0	0.145	-1
	150	0.144	
5.0	0	0.114	0
	150	0.114	

Figure 29: Circular dicroism spectra at different pH values (panel A is at pH 7.4; panel B is at pH 6.2; panel C is at pH 5.0). Black lines are in absence and red ones are in presence of manganese chloride 120 or 150 mM. In table are reported the structuring index (*a/b*) and the percentage of variance (*% var*).

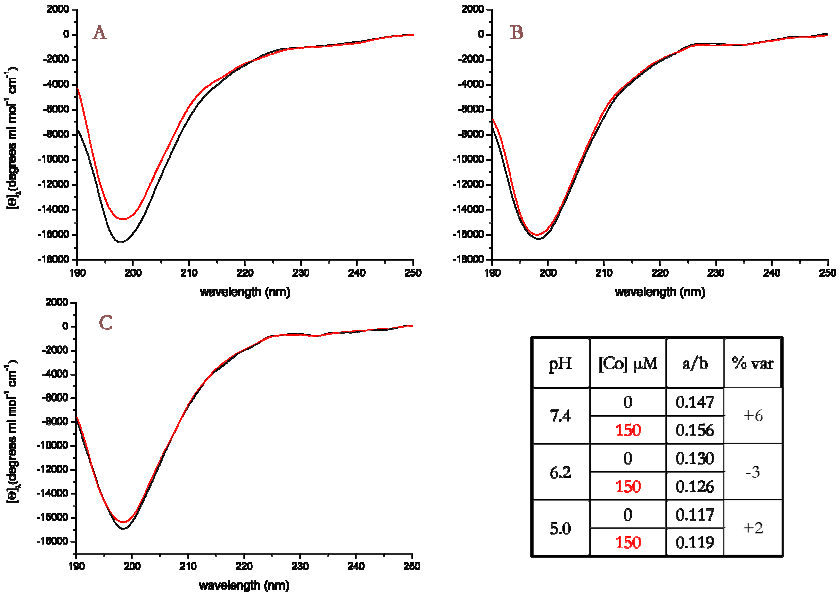

pH	[Co] μM	a/b	% var
7.4	0	0.147	+6
	150	0.156	
6.2	0	0.130	-3
	150	0.126	
5.0	0	0.117	+2
	150	0.119	

Figure 30: Circular dicroism spectra at different pH values (panel A is at pH 7.4; panel B is at pH 6.2; panel C is at pH 5.0). Black lines are in absence and red ones are in presence of cobalt chloride 150 mM. In table are reported the structuring index (*a/b*) and the percentage of variance (*% var*).

4.4. Vitamin PrP$^{23-109}$ binding

Vitamin titrations in fluorescence anisotropy were made as described in §3.11.2.

To check mPrP$^{23-109}$ interaction with vitamins, tryptophan fluorescence anisotropy was evaluated. Fluorescence anisotropy measurements can investigate molecular motion speed; so if tryptophans interact with vitamins, their mobility decreases and, accordingly, their fluorescence anisotropy increases.

Figures 31 to 34 show experimental data of mPrP$^{23-109}$ titrated with vitamins, listed in table 9, at pH 7.4 and in presence of copper 80 μM.

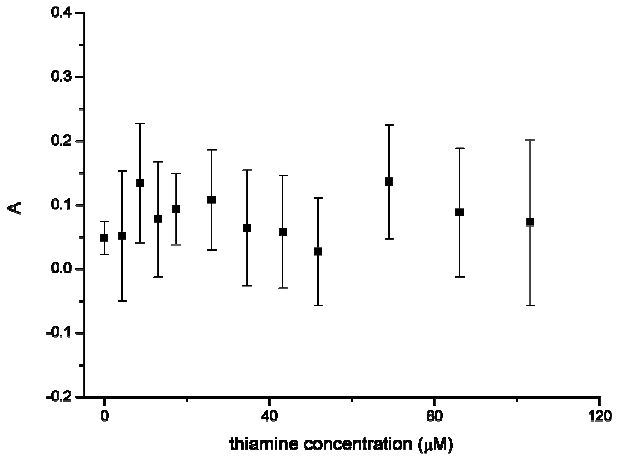

Figure 31: Tryptophan fluorescence anisotropy as function of thiamine concentration.

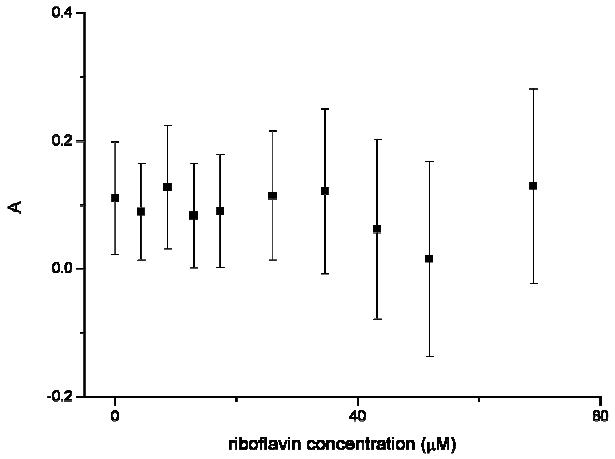

Figure 32: Tryptophan fluorescence anisotropy as function of riboflavin concentration.

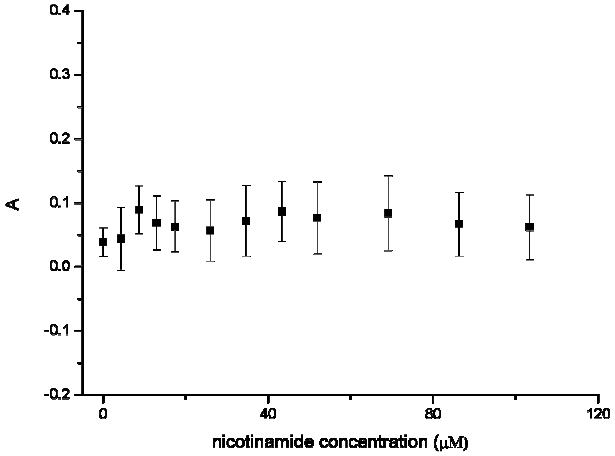

Figure 33: Tryptophan fluorescence anisotropy as function of nicotinamide concentration.

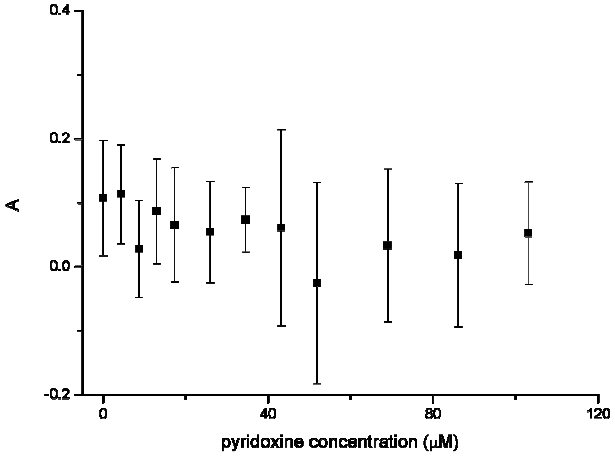

Figure 34: Tryptophan fluorescence anisotropy as function of pyridoxine concentration.

4.5. Membrane mimetic system PrP^{23-109} binding

Neutral vesicles were prepared as described in §3.12.1.1.

Figures 35 shows DMPC liposomes. Vesicles result uniform, unilamellar and their diameter varies from 40 to 100 nm. Changing of pH, presence of protein or metals do not influence vesicles features.

Negatively charged vesicles were prepared as described in §3.12.1.2.

Figures 36 shows DOPG liposomes. Vesicles result less uniform than neutral ones, but they are unilamellar and their diameter varies from 50 to 200 nm. Like for neutral liposomes, changing of pH, presence of protein or metals do not influence vesicles features.

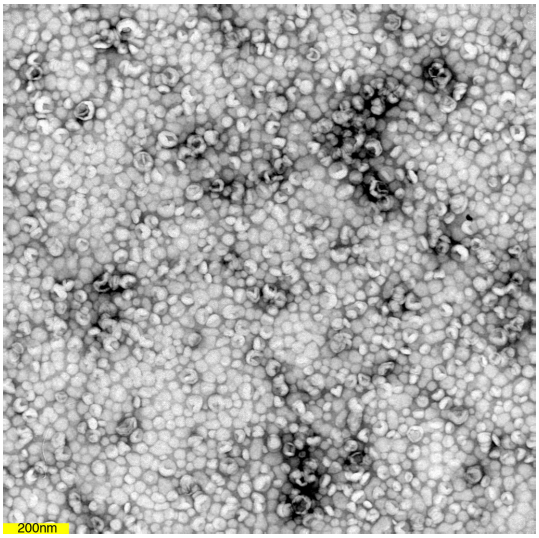

Figure 35: DMPC liposomes.

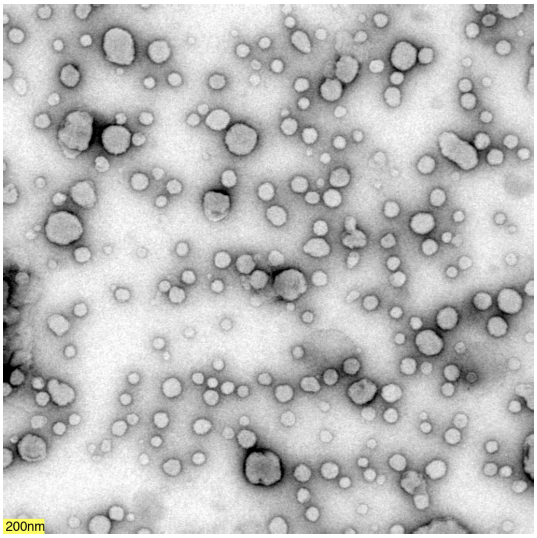

Figure 36: DOPG liposomes.

To check $mPrP^{23-109}$ interaction with membrane mimetic systems, tryptophan fluorescence was evaluated. If tryptophans interact with vesicles, hydrophobic environment, it can be registered a fluorescence blue shift and an increment in fluorescence intensity.

Figure 37 shows fluorescence spectra of $mPrP^{23-109}$ in presence of neutral or charged liposomes. Only negative charged LUVs make fluorescence blue shift.

Figure 38 shows peak wavelength as function of phospholipid concentration. Peak blue shift is of about 6 nm. It is also pH and metal independent.

Neutral or charged liposome titrations do not affect metals binding parameters neither protein structure.

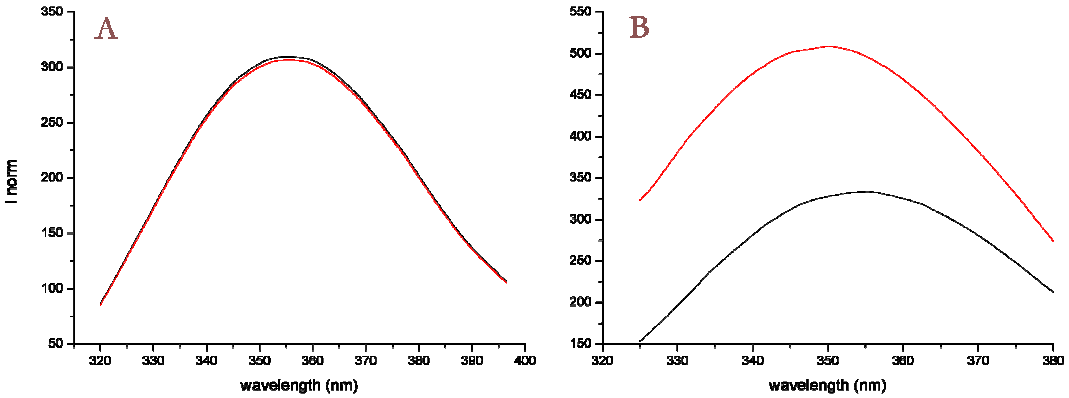

Figure 37: Fluorescence spectra of mPrP$^{23\text{-}109}$ in presence of neutral (panel A) or charged (panel B) liposomes. Black lines are protein only fluorescence spectra; red lines are fluorescence spectra in presence of phospholipids 3 μM.

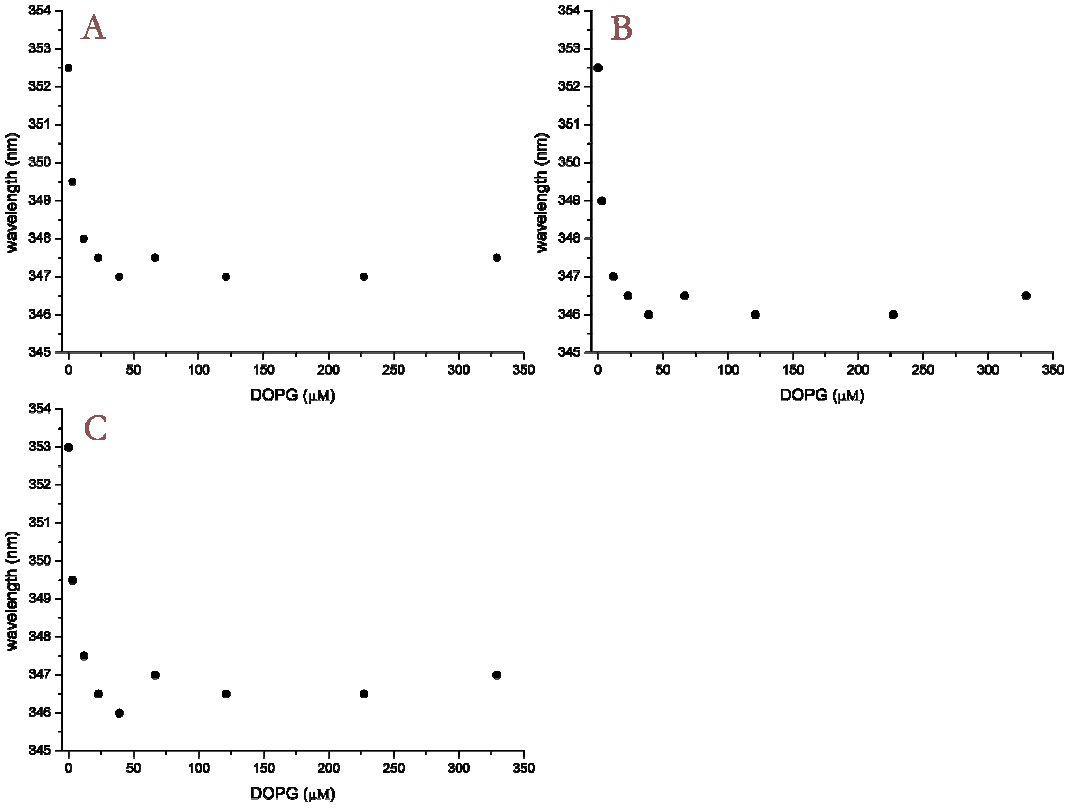

Figure 38: Fluorescence peak wavelength versus phospholipid concentration. In panel A, B and C are showed LUV titrations at pH 7.4, 6.2 and 5.0, respectevely.

5. Discussion and conclusions

Prion protein (PrP^C) is a misundestrood protein. It seems to be involved in some neurodegenerative diseases, but its physiological function is still undefined. Many cellular functions were proposed as PrP^C roles, such as the modulation of several signal transduction pathways known to promote cellular survival[33; 34; 35], the regulation of cell death[28; 29; 30] and the protection against oxidative stress[31; 32]. Nevertheless, the main hypothesis on PrP^C role is in copper homeostasis.

Our hypothesis on PrP^C is based on the copper capabilities to cooperatively bind PrP^C [6; 7; 8], decreasing its over expression[148], stimulating its endocytosis and cellular traffiking[36; 37; 38; 39] via the promotion of the octarepeats α-helix structuring as well as the stacking of triptophan indolic rings[150].

Considering that deficiency of all essential micronutrints (EMNs) produces overlapping of disease symptoms and signs, and that vitamins uptake occurs via endocytic pathways[151; 152; 153; 154], we hypothesize that prion protein, together with copper, plays a key role in integrated endocytic uptake pathway, involving all EMNs.

In particular we propose an integrated mechanism where copper could be uptaked by the octarepeats histidine cooperative binding, while vitamins could be uptaked by octarepeats triptophan binding.

In order to study these binding processes and their characteristics, the N-terminal domain of mouse PrP^C ($mPrP^{23-109}$) was cloned in the expression vector pEt-14b. Once expressed and purified by His-tag affinity chromatography, $mPrP^{23-109}$ has been characterized by SDS-PAGE and ESI mass spectrometry. Recombinant N-terminal domain has a calculated molecular mass of 9154.8 Da (ExPASy ProtParam tool) that it is confirmed by both techniques.

To study specificity and characteristics of metals binding process, $mPrP^{23-109}$ was titrated with five first transition serie divalent metals (Mn, Co, Ni, Cu, Zn), at several pH values in fluorescence spectroscopy. To fit data, we considered first that prion protein metal binding is a cooperative process, accordingly we determined the

saturaction fraction of haevy- metal fluorescence quenching effect on the system metal-mPrP$^{23\text{-}109}$ (§3.9.2).

In agreement with findings of other authors, results show that mPrP$^{23\text{-}109}$ binds copper at neutral pH. Dissociation constant (K_d) of this complex is in the micromolar range. Data also show that, at lower pH values, mPrP$^{23\text{-}109}$ has lower affinity for copper, suggesting the histidine involvement in the binding. Results for nickel titrations show that it binds mPrP$^{23\text{-}109}$ and K_d is comparable to that of copper binding. This similarity is in pH dependence too, showing a decrease in affinity. This features suggest that also nickel could be bond by histidines. Zinc, manganese and cobalt titrations show that all these metals bind the recombinant polypeptide with copper like affinity, but K_d does not vary following buffer acidification.

Data fitting provides also the Hill number. Results show anti-cooperative binding (negative cooperation) for all the considered metals. These results are in contrast with those found in the literature. In fact, we found that glycine in the buffer, a weak copper binding ligand, decreases copper affinity for mPrP$^{23\text{-}109}$ and that even in presence of glycine, Hill number values are less than one. These results can be explained because, in physiological conditions, PrP^{C} is a directed protein, linked to membrane by GPI anchor and stretched towards the extracellular space by glycosilations (Figure 1). On the contrary, in our experiments, recombinant mPrP$^{23\text{-}109}$ is free moving, without constraints. It is clear that in physiological conditions freedom degrees of the N-terminal domain are much lesser than in our experiments, and this may determin changes in some physical features.

In order to define if metal binding could drive structural rearrangements in the prion protein N-terminal domain, we performed structural analysis using Cyrcular Dicroism (CD) spectroscopy. Data interpretation is described in §3.10.2. Briefly, in each CD spectrum values at 222 nm (α-helix index) and 198 nm (random coil index) were used to define a third structural index (*S*); if addition of metals increases the *S* value, it means that metal induces the structuring of protein chain; otherwise, if *S* value decreases, metal induces de-structuring of protein chain. Accordingly to literature[4], CD spectrum of mPrP$^{23\text{-}109}$ in absence of metals is proper of a random

coiled polypeptide. Adding copper at neutral and slightly acid pH, *S* value varies positively, suggesting that copper promotes the protein structuring. Accordingly to fluorescence data, at low pH copper has not effects on protein structure. Nickel titrations show that at neutral and slightly acid pH the structural index decreases of about 20%, indicating that nickel binding destructures the protein. At acidic pH nickel has no effects on protein structure, as showed also for copper. Zinc titrations reveal that it promotes the structuring of protein, in a pH independent manner. Finally, results for manganese and cobalt titrations show that these metals have no effects on protein structure throughout the pH range.

We hypothesize that vitamins could stack between parallel triptophan indolic rings, stacking being induced by copper binding on octarepeat region. To investigate this hypothesis, we performed vitamins titration of $mPrP^{23-109}$, following it by fluorescence anisotropy, that allows to know the fluorophores average molecular rotational speed. If vitamins interacts with protein, their rotational speed decreases, with the consequently increase of fluorescence anisotropy. We found that no one of the examined vitamins alters protein anisotropy, suggesting that there is no interaction with the triptophan indolic rings nor with the rest of the protein.

We also considered the possibility that prion protein N-terminal domain could interact with plasma membrane. To choose the membrane mimetic systems we considered that lipid raft domains are mainly composed by sphingolipids, cholesterol and, to a lesser extent, by phosphatidylcholine, phosphatidylethanolamine and phosphatidylserine[159]. The choosed membrane mimetic systems were: A) not charged (DMPC), B) negatively charged (DOPG). Disposing of two different optimized protocols to prepare large unilamellar vesicles (LUVs), we performed LUVs titration of $mPrP^{23-109}$ monitored by fluorescence spectroscopy, at several pH and in presence or absence of copper. In the case where tryptophans may interact with vesicles hydrophobic environment, a blue shift of the peak wavelength and an increment in fluorescence intensity will be registered. We found that $mPrP^{23-109}$ interacts with negative charged liposomes, but not with neutral ones. Furthermore, still in presence of DOPG 50 μM, a peak wavelength shift of about six nanometers has been

detected. This interaction results to be both metal and pH independent; furthermore neutral or charged LUVs do not affect metal binding parameters nor protein structure, implying that prion protein N-terminal domain could permanently associate with membranes.

We need more investigations to define the prion protein relationships with nickel and zinc, but also to further verify the hypothesized connection between metallic and non metallic micronutrients.

Our findings confirm that prion protein has a functional role in copper homeostasis. We propose a model in which prion protein binds copper in the extracellular medium (pH 7.4), where copper is present as Cu(II) and at very low concentration to Ctr1 binding. Copper binding to PrP^C stimulates endocytosis via early endosomes. We hypothesize that in these intracellular vesicules there are also the Ctr1 copper channels. When early endosomes become late endosomes and lysosomes, lumen pH is lowered by the proton pumps[163]. Acidification promotes copper reduction and copper prion protein affinity decreasing, that cause the copper release into the vesicle lumen. At this point, copper is reduced and more concentrated than extracellular and it can be bind by Ctr1, that traslocates it in the cytoplasmatic side of the vesicle. Here the copper chaperones can transport it to the relative compartments of the cell.

Inside cells, cytoplasmatic precursor of PrP^C is present as a small fraction in comparison with that expressed on cell surface. This precursor is playing the function of sensor and controller of cytosolic Cu concentration. The mechanism is based on the chain structuring effect of copper cooperative bonding on octarepeats that, actually, it selects only two forms of cytosolic precursor PrP, linked by a Cu dependent dynamic equilibrium, the Cu-saturated and the Cu-free form. The last one is the only one susceptible to proteolitic attack by cytosolic proteases[164]. A defect of copper in the cytosol moves the equilibrium towards the Cu-free form, favoring the proteolitic attack that, occurring at the end of octarepeats region, liberates the C–terminal domain. It is notewhorty that C–terminal domain sequence, expecially the tertiary structure, is very strictly conserved from fish up to human, as is occurring for

proteins involved in the protein synthesis process. We propose that the C–terminal domain of cytosolic precursor-PrP is the transcription factor which regulate the over expression of PrP as a conseguence of cytosolic Cu-deficiency.

6. References

1. Prusiner, S. B. (1998). Prions. *Proc Natl Acad Sci U S A* **95**, 13363-83.
2. Stahl, N. & Prusiner, S. B. (1991). Prions and prion proteins. *Faseb J* **5**, 2799-807.
3. Stahl, N., Borchelt, D. R., Hsiao, K. & Prusiner, S. B. (1987). Scrapie prion protein contains a phosphatidylinositol glycolipid. *Cell* **51**, 229-40.
4. Donne, D. G., Viles, J. H., Groth, D., Mehlhorn, I., James, T. L., Cohen, F. E., Prusiner, S. B., Wright, P. E. & Dyson, H. J. (1997). Structure of the recombinant full-length hamster prion protein PrP(29-231): the N terminus is highly flexible. *Proc Natl Acad Sci U S A* **94**, 13452-7.
5. Viles, J. H., Donne, D., Kroon, G., Prusiner, S. B., Cohen, F. E., Dyson, H. J. & Wright, P. E. (2001). Local structural plasticity of the prion protein. Analysis of NMR relaxation dynamics. *Biochemistry* **40**, 2743-53.
6. Brown, D. R., Qin, K., Herms, J. W., Madlung, A., Manson, J., Strome, R., Fraser, P. E., Kruck, T., von Bohlen, A., Schulz-Schaeffer, W., Giese, A., Westaway, D. & Kretzschmar, H. (1997). The cellular prion protein binds copper in vivo. *Nature* **390**, 684-7.
7. Jones, C. E., Klewpatinond, M., Abdelraheim, S. R., Brown, D. R. & Viles, J. H. (2005). Probing copper2+ binding to the prion protein using diamagnetic nickel2+ and 1H NMR: the unstructured N terminus facilitates the coordination of six copper2+ ions at physiological concentrations. *J Mol Biol* **346**, 1393-407.
8. Viles, J. H., Cohen, F. E., Prusiner, S. B., Goodin, D. B., Wright, P. E. & Dyson, H. J. (1999). Copper binding to the prion protein: structural implications of four identical cooperative binding sites. *Proc Natl Acad Sci U S A* **96**, 2042-7.
9. Jones, C. E., Abdelraheim, S. R., Brown, D. R. & Viles, J. H. (2004). Preferential Cu2+ coordination by His96 and His111 induces beta-sheet formation in the unstructured amyloidogenic region of the prion protein. *J Biol Chem* **279**, 32018-27.
10. Jackson, G. S., Murray, I., Hosszu, L. L., Gibbs, N., Waltho, J. P., Clarke, A. R. & Collinge, J. (2001). Location and properties of metal-binding sites on the human prion protein. *Proc Natl Acad Sci U S A* **98**, 8531-5.
11. Hasnain, S. S., Murphy, L. M., Strange, R. W., Grossmann, J. G., Clarke, A. R., Jackson, G. S. & Collinge, J. (2001). XAFS study of the high-affinity copper-binding site of human PrP(91-231) and its low-resolution structure in solution. *J Mol Biol* **311**, 467-73.
12. Burns, C. S., Aronoff-Spencer, E., Legname, G., Prusiner, S. B., Antholine, W. E., Gerfen, G. J., Peisach, J. & Millhauser, G. L. (2003).

Copper coordination in the full-length, recombinant prion protein. *Biochemistry* **42**, 6794-803.
13. Klewpatinond, M. & Viles, J. H. (2007). Fragment length influences affinity for Cu2+ and Ni2+ binding to His96 or His111 of the prion protein and spectroscopic evidence for a multiple histidine binding only at low pH. *Biochem J* **404**, 393-402.
14. Riek, R., Hornemann, S., Wider, G., Billeter, M., Glockshuber, R. & Wuthrich, K. (1996). NMR structure of the mouse prion protein domain PrP(121-321). *Nature* **382**, 180-2.
15. Riek, R., Hornemann, S., Wider, G., Glockshuber, R. & Wuthrich, K. (1997). NMR characterization of the full-length recombinant murine prion protein, mPrP(23-231). *FEBS Lett* **413**, 282-8.
16. Kretzschmar, H. A., Prusiner, S. B., Stowring, L. E. & DeArmond, S. J. (1986). Scrapie prion proteins are synthesized in neurons. *Am J Pathol* **122**, 1-5.
17. Moser, M., Colello, R. J., Pott, U. & Oesch, B. (1995). Developmental expression of the prion protein gene in glial cells. *Neuron* **14**, 509-17.
18. Horiuchi, M., Yamazaki, N., Ikeda, T., Ishiguro, N. & Shinagawa, M. (1995). A cellular form of prion protein (PrPC) exists in many non-neuronal tissues of sheep. *J Gen Virol* **76 (Pt 10)**, 2583-7.
19. Mironov, A., Jr., Latawiec, D., Wille, H., Bouzamondo-Bernstein, E., Legname, G., Williamson, R. A., Burton, D., DeArmond, S. J., Prusiner, S. B. & Peters, P. J. (2003). Cytosolic prion protein in neurons. *J Neurosci* **23**, 7183-93.
20. Vey, M., Pilkuhn, S., Wille, H., Nixon, R., DeArmond, S. J., Smart, E. J., Anderson, R. G., Taraboulos, A. & Prusiner, S. B. (1996). Subcellular colocalization of the cellular and scrapie prion proteins in caveolae-like membranous domains. *Proc Natl Acad Sci U S A* **93**, 14945-9.
21. Peters, P. J., Mironov, A., Jr., Peretz, D., van Donselaar, E., Leclerc, E., Erpel, S., DeArmond, S. J., Burton, D. R., Williamson, R. A., Vey, M. & Prusiner, S. B. (2003). Trafficking of prion proteins through a caveolae-mediated endosomal pathway. *J Cell Biol* **162**, 703-17.
22. Nichols, B. (2003). Caveosomes and endocytosis of lipid rafts. *J Cell Sci* **116**, 4707-14.
23. Schnitzer, J. E., Oh, P., Pinney, E. & Allard, J. (1994). Filipin-sensitive caveolae-mediated transport in endothelium: reduced transcytosis, scavenger endocytosis, and capillary permeability of select macromolecules. *J Cell Biol* **127**, 1217-32.
24. Sunyach, C., Jen, A., Deng, J., Fitzgerald, K. T., Frobert, Y., Grassi, J., McCaffrey, M. W. & Morris, R. (2003). The mechanism of internalization of glycosylphosphatidylinositol-anchored prion protein. *EMBO J* **22**, 3591-601.

25. Magalhaes, A. C., Silva, J. A., Lee, K. S., Martins, V. R., Prado, V. F., Ferguson, S. S., Gomez, M. V., Brentani, R. R. & Prado, M. A. (2002). Endocytic intermediates involved with the intracellular trafficking of a fluorescent cellular prion protein. *J Biol Chem* **277**, 33311-8.
26. Rivera-Milla, E., Oidtmann, B., Panagiotidis, C. H., Baier, M., Sklaviadis, T., Hoffmann, R., Zhou, Y., Solis, G. P., Stuermer, C. A. & Malaga-Trillo, E. (2006). Disparate evolution of prion protein domains and the distinct origin of Doppel- and prion-related loci revealed by fish-to-mammal comparisons. *Faseb J* **20**, 317-9.
27. Rivera-Milla, E., Stuermer, C. A. & Malaga-Trillo, E. (2003). An evolutionary basis for scrapie disease: identification of a fish prion mRNA. *Trends Genet* **19**, 72-5.
28. Kuwahara, C., Takeuchi, A. M., Nishimura, T., Haraguchi, K., Kubosaki, A., Matsumoto, Y., Saeki, K., Yokoyama, T., Itohara, S. & Onodera, T. (1999). Prions prevent neuronal cell-line death. *Nature* **400**, 225-6.
29. Bounhar, Y., Zhang, Y., Goodyer, C. G. & LeBlanc, A. (2001). Prion protein protects human neurons against Bax-mediated apoptosis. *J Biol Chem* **276**, 39145-9.
30. Paitel, E., Sunyach, C., Alves da Costa, C., Bourdon, J. C., Vincent, B. & Checler, F. (2004). Primary cultured neurons devoid of cellular prion display lower responsiveness to staurosporine through the control of p53 at both transcriptional and post-transcriptional levels. *J Biol Chem* **279**, 612-8.
31. Brown, D. R., Schulz-Schaeffer, W. J., Schmidt, B. & Kretzschmar, H. A. (1997). Prion protein-deficient cells show altered response to oxidative stress due to decreased SOD-1 activity. *Exp Neurol* **146**, 104-12.
32. Wong, B. S., Liu, T., Li, R., Pan, T., Petersen, R. B., Smith, M. A., Gambetti, P., Perry, G., Manson, J. C., Brown, D. R. & Sy, M. S. (2001). Increased levels of oxidative stress markers detected in the brains of mice devoid of prion protein. *J Neurochem* **76**, 565-72.
33. Mouillet-Richard, S., Ermonval, M., Chebassier, C., Laplanche, J. L., Lehmann, S., Launay, J. M. & Kellermann, O. (2000). Signal transduction through prion protein. *Science* **289**, 1925-8.
34. Chiarini, L. B., Freitas, A. R., Zanata, S. M., Brentani, R. R., Martins, V. R. & Linden, R. (2002). Cellular prion protein transduces neuroprotective signals. *EMBO J* **21**, 3317-26.
35. Zanata, S. M., Lopes, M. H., Mercadante, A. F., Hajj, G. N., Chiarini, L. B., Nomizo, R., Freitas, A. R., Cabral, A. L., Lee, K. S., Juliano, M. A., de Oliveira, E., Jachieri, S. G., Burlingame, A., Huang, L., Linden, R., Brentani, R. R. & Martins, V. R. (2002). Stress-inducible protein 1 is a cell surface ligand for cellular prion that triggers neuroprotection. *EMBO J* **21**, 3307-16.

36. Brown, L. R. & Harris, D. A. (2003). Copper and zinc cause delivery of the prion protein from the plasma membrane to a subset of early endosomes and the Golgi. *J Neurochem* **87**, 353-63.
37. Lee, K. S., Magalhaes, A. C., Zanata, S. M., Brentani, R. R., Martins, V. R. & Prado, M. A. (2001). Internalization of mammalian fluorescent cellular prion protein and N-terminal deletion mutants in living cells. *J Neurochem* **79**, 79-87.
38. Pauly, P. C. & Harris, D. A. (1998). Copper stimulates endocytosis of the prion protein. *J Biol Chem* **273**, 33107-10.
39. Perera, W. S. & Hooper, N. M. (2001). Ablation of the metal ion-induced endocytosis of the prion protein by disease-associated mutation of the octarepeat region. *Curr Biol* **11**, 519-23.
40. Wong, B. S., Chen, S. G., Colucci, M., Xie, Z., Pan, T., Liu, T., Li, R., Gambetti, P., Sy, M. S. & Brown, D. R. (2001). Aberrant metal binding by prion protein in human prion disease. *J Neurochem* **78**, 1400-8.
41. Brown, D. R., Nicholas, R. S. & Canevari, L. (2002). Lack of prion protein expression results in a neuronal phenotype sensitive to stress. *J Neurosci Res* **67**, 211-24.
42. Herms, J., Tings, T., Gall, S., Madlung, A., Giese, A., Siebert, H., Schurmann, P., Windl, O., Brose, N. & Kretzschmar, H. (1999). Evidence of presynaptic location and function of the prion protein. *J Neurosci* **19**, 8866-75.
43. Opazo, C., Barria, M. I., Ruiz, F. H. & Inestrosa, N. C. (2003). Copper reduction by copper binding proteins and its relation to neurodegenerative diseases. *Biometals* **16**, 91-8.
44. Ruiz, F. H., Silva, E. & Inestrosa, N. C. (2000). The N-terminal tandem repeat region of human prion protein reduces copper: role of tryptophan residues. *Biochem Biophys Res Commun* **269**, 491-5.
45. Nadal, R. C., Abdelraheim, S. R., Brazier, M. W., Rigby, S. E., Brown, D. R. & Viles, J. H. (2007). Prion protein does not redox-silence Cu2+, but is a sacrificial quencher of hydroxyl radicals. *Free Radic Biol Med* **42**, 79-89.
46. Tallkvist, J., Bowlus, C. L. & Lonnerdal, B. (2000). Functional and molecular responses of human intestinal Caco-2 cells to iron treatment. *Am J Clin Nutr* **72**, 770-5.
47. Leblondel, G. & Allain, P. (1999). Manganese transport by Caco-2 cells. *Biol Trace Elem Res* **67**, 13-28.
48. Gunshin, H., Mackenzie, B., Berger, U. V., Gunshin, Y., Romero, M. F., Boron, W. F., Nussberger, S., Gollan, J. L. & Hediger, M. A. (1997). Cloning and characterization of a mammalian proton-coupled metal-ion transporter. *Nature* **388**, 482-8.
49. Chua, A. C. & Morgan, E. H. (1997). Manganese metabolism is impaired in the Belgrade laboratory rat. *J Comp Physiol [B]* **167**, 361-9.

50. Crossgrove, J. S. & Yokel, R. A. (2004). Manganese distribution across the blood-brain barrier III. The divalent metal transporter-1 is not the major mechanism mediating brain manganese uptake. *Neurotoxicology* **25**, 451-60.
51. Aschner, M., Shanker, G., Erikson, K., Yang, J. & Mutkus, L. A. (2002). The uptake of manganese in brain endothelial cultures. *Neurotoxicology* **23**, 165-8.
52. Aschner, M., Gannon, M. & Kimelberg, H. K. (1992). Manganese uptake and efflux in cultured rat astrocytes. *J Neurochem* **58**, 730-5.
53. Erikson, K. M. & Aschner, M. (2006). Increased manganese uptake by primary astrocyte cultures with altered iron status is mediated primarily by divalent metal transporter. *Neurotoxicology* **27**, 125-30.
54. Crossgrove, J. S., Allen, D. D., Bukaveckas, B. L., Rhineheimer, S. S. & Yokel, R. A. (2003). Manganese distribution across the blood-brain barrier. I. Evidence for carrier-mediated influx of managanese citrate as well as manganese and manganese transferrin. *Neurotoxicology* **24**, 3-13.
55. Murphy, V. A., Wadhwani, K. C., Smith, Q. R. & Rapoport, S. I. (1991). Saturable transport of manganese(II) across the rat blood-brain barrier. *J Neurochem* **57**, 948-54.
56. Rabin, O., Hegedus, L., Bourre, J. M. & Smith, Q. R. (1993). Rapid brain uptake of manganese(II) across the blood-brain barrier. *J Neurochem* **61**, 509-17.
57. Davidsson, L., Lonnerdal, B., Sandstrom, B., Kunz, C. & Keen, C. L. (1989). Identification of transferrin as the major plasma carrier protein for manganese introduced orally or intravenously or after in vitro addition in the rat. *J Nutr* **119**, 1461-4.
58. Davis, C. D. & Greger, J. L. (1992). Longitudinal changes of manganese-dependent superoxide dismutase and other indexes of manganese and iron status in women. *Am J Clin Nutr* **55**, 747-52.
59. Rossander-Hulten, L., Brune, M., Sandstrom, B., Lonnerdal, B. & Hallberg, L. (1991). Competitive inhibition of iron absorption by manganese and zinc in humans. *Am J Clin Nutr* **54**, 152-6.
60. Wedler, F. C. & Denman, R. B. (1984). Glutamine synthetase: the major Mn(II) enzyme in mammalian brain. *Curr Top Cell Regul* **24**, 153-69.
61. Davis, C. D., Zech, L. & Greger, J. L. (1993). Manganese metabolism in rats: an improved methodology for assessing gut endogenous losses. *Proc Soc Exp Biol Med* **202**, 103-8.
62. Kobayashi, M. & Shimizu, S. (1999). Cobalt proteins. *Eur J Biochem* **261**, 1-9.
63. Addlagatta, A., Hu, X., Liu, J. O. & Matthews, B. W. (2005). Structural basis for the functional differences between type I and type II human methionine aminopeptidases. *Biochemistry* **44**, 14741-9.

64. Arfin, S. M., Kendall, R. L., Hall, L., Weaver, L. H., Stewart, A. E., Matthews, B. W. & Bradshaw, R. A. (1995). Eukaryotic methionyl aminopeptidases: two classes of cobalt-dependent enzymes. *Proc Natl Acad Sci U S A* **92**, 7714-8.
65. Krautler, B. (2005). Vitamin B12: chemistry and biochemistry. *Biochem Soc Trans* **33**, 806-10.
66. Smith, T. A. (2005). Human serum transferrin cobalt complex: stability and cellular uptake of cobalt. *Bioorg Med Chem* **13**, 4576-9.
67. Uthus, E. O. & Seaborn, C. D. (1996). Deliberations and evaluations of the approaches, endpoints and paradigms for dietary recommendations of the other trace elements. *J Nutr* **126**, 2452S-2459S.
68. Kim, H., Yu, C. & Maier, R. J. (1991). Common cis-acting region responsible for transcriptional regulation of Bradyrhizobium japonicum hydrogenase by nickel, oxygen, and hydrogen. *J Bacteriol* **173**, 3993-9.
69. Przybyla, A. E., Robbins, J., Menon, N. & Peck, H. D., Jr. (1992). Structure-function relationships among the nickel-containing hydrogenases. *FEMS Microbiol Rev* **8**, 109-35.
70. Nielsen, F. H. (1985). The importance of diet composition in ultratrace element research. *J Nutr* **115**, 1239-47.
71. Schnegg, A. & Kirchgessner, M. (1975). [Changes in hemoglobin content, erythrocyte count and hematocrit in nickel deficiency]. *Nutr Metab* **19**, 268-78.
72. Nielsen, F. H. (1996). How should dietary guidance be given for mineral elements with beneficial actions or suspected of being essential? *J Nutr* **126**, 2377S-2385S.
73. Uthus, E. O. & Poellot, R. A. (1996). Dietary folate affects the response of rats to nickel deprivation. *Biol Trace Elem Res* **52**, 23-35.
74. Solomons, N. W., Viteri, F., Shuler, T. R. & Nielsen, F. H. (1982). Bioavailability of nickel in man: effects of foods and chemically-defined dietary constituents on the absorption of inorganic nickel. *J Nutr* **112**, 39-50.
75. Tallkvist, J., Wing, A. M. & Tjalve, H. (1994). Enhanced intestinal nickel absorption in iron-deficient rats. *Pharmacol Toxicol* **75**, 244-9.
76. Tallkvist, J. & Tjalve, H. (1997). Effect of dietary iron-deficiency on the disposition of nickel in rats. *Toxicol Lett* **92**, 131-8.
77. Tallkvist, J. & Tjalve, H. (1998). Transport of nickel across monolayers of human intestinal Caco-2 cells. *Toxicol Appl Pharmacol* **151**, 117-22.
78. Tallkvist, J., Bowlus, C. L. & Lonnerdal, B. (2003). Effect of iron treatment on nickel absorption and gene expression of the divalent metal transporter (DMT1) by human intestinal Caco-2 cells. *Pharmacol Toxicol* **92**, 121-4.

79. Tabata, M. & Sarkar, B. (1992). Specific nickel(II)-transfer process between the native sequence peptide representing the nickel(II)-transport site of human serum albumin and L-histidine. *J Inorg Biochem* **45**, 93-104.
80. Rezuke, W. N., Knight, J. A. & Sunderman, F. W., Jr. (1987). Reference values for nickel concentrations in human tissues and bile. *Am J Ind Med* **11**, 419-26.
81. Linder, M. C. & Hazegh-Azam, M. (1996). Copper biochemistry and molecular biology. *Am J Clin Nutr* **63**, 797S-811S.
82. Harris, Z. L. & Gitlin, J. D. (1996). Genetic and molecular basis for copper toxicity. *Am J Clin Nutr* **63**, 836S-41S.
83. Milne, D. B. (1994). Assessment of copper nutritional status. *Clin Chem* **40**, 1479-84.
84. Graham, G. G. & Cordano, A. (1969). Copper depletion and deficiency in the malnourished infant. *Johns Hopkins Med J* **124**, 139-50.
85. Olivares, M. & Uauy, R. (1996). Limits of metabolic tolerance to copper and biological basis for present recommendations and regulations. *Am J Clin Nutr* **63**, 846S-52S.
86. Turnlund, J. R. (1998). Human whole-body copper metabolism. *Am J Clin Nutr* **67**, 960S-964S.
87. Puig, S., Lee, J., Lau, M. & Thiele, D. J. (2002). Biochemical and genetic analyses of yeast and human high affinity copper transporters suggest a conserved mechanism for copper uptake. *J Biol Chem* **277**, 26021-30.
88. Puig, S. & Thiele, D. J. (2002). Molecular mechanisms of copper uptake and distribution. *Curr Opin Chem Biol* **6**, 171-80.
89. Petris, M. J. (2004). The SLC31 (Ctr) copper transporter family. *Pflugers Arch* **447**, 752-5.
90. Lee, J., Pena, M. M., Nose, Y. & Thiele, D. J. (2002). Biochemical characterization of the human copper transporter Ctr1. *J Biol Chem* **277**, 4380-7.
91. Kuo, Y. M., Zhou, B., Cosco, D. & Gitschier, J. (2001). The copper transporter CTR1 provides an essential function in mammalian embryonic development. *Proc Natl Acad Sci U S A* **98**, 6836-41.
92. Lee, J., Prohaska, J. R. & Thiele, D. J. (2001). Essential role for mammalian copper transporter Ctr1 in copper homeostasis and embryonic development. *Proc Natl Acad Sci U S A* **98**, 6842-7.
93. Klomp, A. E., Tops, B. B., Van Denberg, I. E., Berger, R. & Klomp, L. W. (2002). Biochemical characterization and subcellular localization of human copper transporter 1 (hCTR1). *Biochem J* **364**, 497-505.
94. Lee, J., Petris, M. J. & Thiele, D. J. (2002). Characterization of mouse embryonic cells deficient in the ctr1 high affinity copper transporter. Identification of a Ctr1-independent copper transport system. *J Biol Chem* **277**, 40253-9.

95. Pena, M. M., Lee, J. & Thiele, D. J. (1999). A delicate balance: homeostatic control of copper uptake and distribution. *J Nutr* **129**, 1251-60.
96. Vallee, B. L. & Galdes, A. (1984). The metallobiochemistry of zinc enzymes. *Adv Enzymol Relat Areas Mol Biol* **56**, 283-430.
97. Klug, A. & Schwabe, J. W. (1995). Protein motifs 5. Zinc fingers. *Faseb J* **9**, 597-604.
98. Huse, M., Eck, M. J. & Harrison, S. C. (1998). A Zn2+ ion links the cytoplasmic tail of CD4 and the N-terminal region of Lck. *J Biol Chem* **273**, 18729-33.
99. Lin, R. S., Rodriguez, C., Veillette, A. & Lodish, H. F. (1998). Zinc is essential for binding of p56(lck) to CD4 and CD8alpha. *J Biol Chem* **273**, 32878-82.
100. Cousins, R. J. (1989). Theoretical and practical aspects of zinc uptake and absorption. *Adv Exp Med Biol* **249**, 3-12.
101. Lee, H. H., Prasad, A. S., Brewer, G. J. & Owyang, C. (1989). Zinc absorption in human small intestine. *Am J Physiol* **256**, G87-91.
102. Eide, D. J. (2004). The SLC39 family of metal ion transporters. *Pflugers Arch* **447**, 796-800.
103. Palmiter, R. D. & Huang, L. (2004). Efflux and compartmentalization of zinc by members of the SLC30 family of solute carriers. *Pflugers Arch* **447**, 744-51.
104. Liuzzi, J. P. & Cousins, R. J. (2004). Mammalian zinc transporters. *Annu Rev Nutr* **24**, 151-72.
105. Ishihara, K., Yamazaki, T., Ishida, Y., Suzuki, T., Oda, K., Nagao, M., Yamaguchi-Iwai, Y. & Kambe, T. (2006). Zinc transport complexes contribute to the homeostatic maintenance of secretory pathway function in vertebrate cells. *J Biol Chem* **281**, 17743-50.
106. Van Eerdewegh, P., Little, R. D., Dupuis, J., Del Mastro, R. G., Falls, K., Simon, J., Torrey, D., Pandit, S., McKenny, J., Braunschweiger, K., Walsh, A., Liu, Z., Hayward, B., Folz, C., Manning, S. P., Bawa, A., Saracino, L., Thackston, M., Benchekroun, Y., Capparell, N., Wang, M., Adair, R., Feng, Y., Dubois, J., FitzGerald, M. G., Huang, H., Gibson, R., Allen, K. M., Pedan, A., Danzig, M. R., Umland, S. P., Egan, R. W., Cuss, F. M., Rorke, S., Clough, J. B., Holloway, J. W., Holgate, S. T. & Keith, T. P. (2002). Association of the ADAM33 gene with asthma and bronchial hyperresponsiveness. *Nature* **418**, 426-30.
107. Chowanadisai, W., Lonnerdal, B. & Kelleher, S. L. (2006). Identification of a mutation in SLC30A2 (ZnT-2) in women with low milk zinc concentration that results in transient neonatal zinc deficiency. *J Biol Chem* **281**, 39699-707.

108. Thirumoorthy, N., Manisenthil Kumar, K. T., Shyam Sundar, A., Panayappan, L. & Chatterjee, M. (2007). Metallothionein: an overview. *World J Gastroenterol* **13**, 993-6.
109. Tallaksen, C. M., Bell, H. & Bohmer, T. (1993). Thiamin and thiamin phosphate ester deficiency assessed by high performance liquid chromatography in four clinical cases of Wernicke encephalopathy. *Alcohol Clin Exp Res* **17**, 712-6.
110. Tomasulo, P. A., Kater, R. M. & Iber, F. L. (1968). Impairment of thiamine absorption in alcoholism. *Am J Clin Nutr* **21**, 1341-4.
111. Dudeja, P. K., Tyagi, S., Kavilaveettil, R. J., Gill, R. & Said, H. M. (2001). Mechanism of thiamine uptake by human jejunal brush-border membrane vesicles. *Am J Physiol Cell Physiol* **281**, C786-92.
112. Dutta, B., Huang, W., Molero, M., Kekuda, R., Leibach, F. H., Devoe, L. D., Ganapathy, V. & Prasad, P. D. (1999). Cloning of the human thiamine transporter, a member of the folate transporter family. *J Biol Chem* **274**, 31925-9.
113. Fleming, J. C., Tartaglini, E., Steinkamp, M. P., Schorderet, D. F., Cohen, N. & Neufeld, E. J. (1999). The gene mutated in thiamine-responsive anaemia with diabetes and deafness (TRMA) encodes a functional thiamine transporter. *Nat Genet* **22**, 305-8.
114. Labay, V., Raz, T., Baron, D., Mandel, H., Williams, H., Barrett, T., Szargel, R., McDonald, L., Shalata, A., Nosaka, K., Gregory, S. & Cohen, N. (1999). Mutations in SLC19A2 cause thiamine-responsive megaloblastic anaemia associated with diabetes mellitus and deafness. *Nat Genet* **22**, 300-4.
115. Rajgopal, A., Edmondnson, A., Goldman, I. D. & Zhao, R. (2001). SLC19A3 encodes a second thiamine transporter ThTr2. *Biochim Biophys Acta* **1537**, 175-8.
116. Davis, R. E., Icke, G. C., Thom, J. & Riley, W. J. (1984). Intestinal absorption of thiamin in man compared with folate and pyridoxal and its subsequent urinary excretion. *J Nutr Sci Vitaminol (Tokyo)* **30**, 475-82.
117. Huang, S. N. & Swaan, P. W. (2000). Involvement of a receptor-mediated component in cellular translocation of riboflavin. *J Pharmacol Exp Ther* **294**, 117-25.
118. Said, H. M. & Ma, T. Y. (1994). Mechanism of riboflavine uptake by Caco-2 human intestinal epithelial cells. *Am J Physiol* **266**, G15-21.
119. Said, H. M., Ortiz, A., Moyer, M. P. & Yanagawa, N. (2000). Riboflavin uptake by human-derived colonic epithelial NCM460 cells. *Am J Physiol Cell Physiol* **278**, C270-6.
120. Huang, S. N., Phelps, M. A. & Swaan, P. W. (2003). Involvement of endocytic organelles in the subcellular trafficking and localization of riboflavin. *J Pharmacol Exp Ther* **306**, 681-7.

121. Said, H. M. & Arianas, P. (1991). Transport of riboflavin in human intestinal brush border membrane vesicles. *Gastroenterology* **100**, 82-8.
122. Rindi, G. & Gastaldi, G. (1997). Measurements and characteristics of intestinal riboflavin transport. *Methods Enzymol* **280**, 399-407.
123. Yonezawa, A., Masuda, S., Katsura, T. & Inui, K. (2008). Identification and functional characterization of a novel human and rat riboflavin transporter, RFT1. *Am J Physiol Cell Physiol* **295**, C632-41.
124. Innis, W. S., McCormick, D. B. & Merrill, A. H., Jr. (1985). Variations in riboflavin binding by human plasma: identification of immunoglobulins as the major proteins responsible. *Biochem Med* **34**, 151-65.
125. Lee, S. S. & McCormick, D. B. (1983). Effect of riboflavin status on hepatic activities of flavin-metabolizing enzymes in rats. *J Nutr* **113**, 2274-9.
126. Yamada, Y., Merrill, A. H., Jr. & McCormick, D. B. (1990). Probable reaction mechanisms of flavokinase and FAD synthetase from rat liver. *Arch Biochem Biophys* **278**, 125-30.
127. McCormick, D. B. (1989). Two interconnected B vitamins: riboflavin and pyridoxine. *Physiol Rev* **69**, 1170-98.
128. Kim, H., Jacobson, E. L. & Jacobson, M. K. (1994). NAD glycohydrolases: a possible function in calcium homeostasis. *Mol Cell Biochem* **138**, 237-43.
129. Lautier, D., Lagueux, J., Thibodeau, J., Menard, L. & Poirier, G. G. (1993). Molecular and biochemical features of poly (ADP-ribose) metabolism. *Mol Cell Biochem* **122**, 171-93.
130. Henderson, L. M. & Gross, C. J. (1979). Transport of niacin and niacinamide in perfused rat intestine. *J Nutr* **109**, 646-53.
131. Simanjuntak, M. T., Tamai, I., Terasaki, T. & Tsuji, A. (1990). Carrier-mediated uptake of nicotinic acid by rat intestinal brush-border membrane vesicles and relation to monocarboxylic acid transport. *J Pharmacobiodyn* **13**, 301-9.
132. Takanaga, H., Maeda, H., Yabuuchi, H., Tamai, I., Higashida, H. & Tsuji, A. (1996). Nicotinic acid transport mediated by pH-dependent anion antiporter and proton cotransporter in rabbit intestinal brush-border membrane. *J Pharm Pharmacol* **48**, 1073-7.
133. Nabokina, S. M., Kashyap, M. L. & Said, H. M. (2005). Mechanism and regulation of human intestinal niacin uptake. *Am J Physiol Cell Physiol* **289**, C97-103.
134. Guggino, S. E. & Aronson, P. S. (1985). Paradoxical effects of pyrazinoate and nicotinate on urate transport in dog renal microvillus membranes. *J Clin Invest* **76**, 543-7.
135. Manganel, M., Roch-Ramel, F. & Murer, H. (1985). Sodium-pyrazinoate cotransport in rabbit renal brush border membrane vesicles. *Am J Physiol* **249**, F400-8.

136. Schuette, S. & Rose, R. C. (1986). Renal transport and metabolism of nicotinic acid. *Am J Physiol* **250**, C694-703.
137. Bernofsky, C. (1980). Physiology aspects of pyridine nucleotide regulation in mammals. *Mol Cell Biochem* **33**, 135-43.
138. Mrochek, J. E., Jolley, R. L., Young, D. S. & Turner, W. J. (1976). Metabolic response of humans to ingestion of nicotinic acid and nicotinamide. *Clin Chem* **22**, 1821-7.
139. Said, H. M., Ortiz, A. & Ma, T. Y. (2003). A carrier-mediated mechanism for pyridoxine uptake by human intestinal epithelial Caco-2 cells: regulation by a PKA-mediated pathway. *Am J Physiol Cell Physiol* **285**, C1219-25.
140. Said, Z. M., Subramanian, V. S., Vaziri, N. D. & Said, H. M. (2008). Pyridoxine uptake by colonocytes: a specific and regulated carrier-mediated process. *Am J Physiol Cell Physiol* **294**, C1192-7.
141. Merrill, A. H., Jr., Henderson, J. M., Wang, E., McDonald, B. W. & Millikan, W. J. (1984). Metabolism of vitamin B-6 by human liver. *J Nutr* **114**, 1664-74.
142. Fonda, M. L., Trauss, C. & Guempel, U. M. (1991). The binding of pyridoxal 5'-phosphate to human serum albumin. *Arch Biochem Biophys* **288**, 79-86.
143. Leklem, J. E. & Shultz, T. D. (1983). Increased plasma pyridoxal 5'-phosphate and vitamin B6 in male adolescents after 4500-meter run. *Am J Clin Nutr* **38**, 541-8.
144. Harris, D. A. & True, H. L. (2006). New insights into prion structure and toxicity. *Neuron* **50**, 353-7.
145. Bueler, H., Fischer, M., Lang, Y., Bluethmann, H., Lipp, H. P., DeArmond, S. J., Prusiner, S. B., Aguet, M. & Weissmann, C. (1992). Normal development and behaviour of mice lacking the neuronal cell-surface PrP protein. *Nature* **356**, 577-82.
146. Manson, J. C., Clarke, A. R., Hooper, M. L., Aitchison, L., McConnell, I. & Hope, J. (1994). 129/Ola mice carrying a null mutation in PrP that abolishes mRNA production are developmentally normal. *Mol Neurobiol* **8**, 121-7.
147. Mallucci, G. R., Ratte, S., Asante, E. A., Linehan, J., Gowland, I., Jefferys, J. G. & Collinge, J. (2002). Post-natal knockout of prion protein alters hippocampal CA1 properties, but does not result in neurodegeneration. *EMBO J* **21**, 202-10.
148. Toni, M., Massimino, M. L., Griffoni, C., Salvato, B., Tomasi, V. & Spisni, E. (2005). Extracellular copper ions regulate cellular prion protein (PrPC) expression and metabolism in neuronal cells. *FEBS Lett* **579**, 741-4.
149. Xiao, Z., Loughlin, F., George, G. N., Howlett, G. J. & Wedd, A. G. (2004). C-terminal domain of the membrane copper transporter Ctr1 from

Saccharomyces cerevisiae binds four Cu(I) ions as a cuprous-thiolate polynuclear cluster: sub-femtomolar Cu(I) affinity of three proteins involved in copper trafficking. *J Am Chem Soc* **126**, 3081-90.

150. Miura, T., Hori-i, A. & Takeuchi, H. (1996). Metal-dependent alpha-helix formation promoted by the glycine-rich octapeptide region of prion protein. *FEBS Lett* **396**, 248-52.
151. Holladay, S. R., Yang, Z., Kennedy, M. D., Leamon, C. P., Lee, R. J., Jayamani, M., Mason, T. & Low, P. S. (1999). Riboflavin-mediated delivery of a macromolecule into cultured human cells. *Biochim Biophys Acta* **1426**, 195-204.
152. Seetharam, B. (1999). Receptor-mediated endocytosis of cobalamin (vitamin B12). *Annu Rev Nutr* **19**, 173-95.
153. Foraker, A. B., Ray, A., Da Silva, T. C., Bareford, L. M., Hillgren, K. M., Schmittgen, T. D. & Swaan, P. W. (2007). Dynamin 2 regulates riboflavin endocytosis in human placental trophoblasts. *Mol Pharmacol* **72**, 553-62.
154. Rothberg, K. G., Ying, Y. S., Kolhouse, J. F., Kamen, B. A. & Anderson, R. G. (1990). The glycophospholipid-linked folate receptor internalizes folate without entering the clathrin-coated pit endocytic pathway. *J Cell Biol* **110**, 637-49.
155. Taylor, J. P., Hardy, J. & Fischbeck, K. H. (2002). Toxic proteins in neurodegenerative disease. *Science* **296**, 1991-5.
156. Harris, D. A., Huber, M. T., van Dijken, P., Shyng, S. L., Chait, B. T. & Wang, R. (1993). Processing of a cellular prion protein: identification of N- and C-terminal cleavage sites. *Biochemistry* **32**, 1009-16.
157. Chen, S. G., Teplow, D. B., Parchi, P., Teller, J. K., Gambetti, P. & Autilio-Gambetti, L. (1995). Truncated forms of the human prion protein in normal brain and in prion diseases. *J Biol Chem* **270**, 19173-80.
158. Vincent, B., Paitel, E., Frobert, Y., Lehmann, S., Grassi, J. & Checler, F. (2000). Phorbol ester-regulated cleavage of normal prion protein in HEK293 human cells and murine neurons. *J Biol Chem* **275**, 35612-6.
159. Michel, V. & Bakovic, M. (2007). Lipid rafts in health and disease. *Biol Cell* **99**, 129-40.
160. Chang, J. Y. (1985). Thrombin specificity. Requirement for apolar amino acids adjacent to the thrombin cleavage site of polypeptide substrate. *Eur J Biochem* **151**, 217-24.
161. Kramer, M. L., Kratzin, H. D., Schmidt, B., Romer, A., Windl, O., Liemann, S., Hornemann, S. & Kretzschmar, H. (2001). Prion protein binds copper within the physiological concentration range. *J Biol Chem* **276**, 16711-9.
162. Kremer, J. M., Esker, M. W., Pathmamanoharan, C. & Wiersema, P. H. (1977). Vesicles of variable diameter prepared by a modified injection method. *Biochemistry* **16**, 3932-5.

163. Gruenberg, J. (2001). The endocytic pathway: a mosaic of domains. *Nat Rev Mol Cell Biol* **2**, 721-30.
164. Quaglio, E., Chiesa, R. & Harris, D. A. (2001). Copper converts the cellular prion protein into a protease-resistant species that is distinct from the scrapie isoform. *J Biol Chem* **276**, 11432-8.